Diploma thesis

Friction Force Microscopy characterization of organic thin films

Quan SHEN

Performed at the

Institute of Physics

University of Leoben, Austria

Under the supervision of

Dipl.-Ing. Dr. mont. Gregor HLAWACEK

Ao. Univ. Prof. Dr. Christian TEICHERT

refereed by

Ao. Univ. Prof. Dr. Christian TEICHERT

Leoben, June 2009

for my mother

EIDESSTATTLICHE ERKLÄRUNG

Ich erkläre an Eides statt, dass ich diese Arbeit selbständig verfasst, andere als die angegebenen Quellen und Hilfsmittel nicht benutzt und mich auch sonst keiner unerlaubten Hilfsmittel bedient habe.

AFFIDAVIT

I declare in lieu of oath, that I wrote this thesis and performed the associated research myself, using only literature cited in this volume.

______________________________ ______________________________

Datum Unterschrift

Abstract

A new class of materials, organic semiconductors, has been developed for novel applications, such as large-area lighting and flexible displays, plastic solar cells or modern low-cost electronic devices. The device performance significantly depends on the properties of the interface layer between the organic semiconductor and the inorganic electric components. The focus in this contribution is put on the surface investigations of three different organic surface layers. Organosilane self-assembled oligolayers, i.e. thin layers of (Heptadecafluoro-1,1,2,2-tetrahydrodecyl) trichloro-silane (PFDTS) and 2-(4-Chlorosulfonylphenyl) ethyltrichlorosilane (CSTS), are investigated. These are typically applied in Organic Thin Film Transistors (OTFTs) as interfacial layers and strongly influence the device performance. Using Atomic Force Microscopy (AFM), surface roughness parameters have been determined. Comparing the surface properties of layers formed by different methods, the preparation method in a glove box turns out to be the best method. Contact Angle measurements were used to follow the chemical modification of the surface. In addition, photosensitive organosilane surface layers - thin layers of (4-thiocyanatomethyl) phenyltrimethoxy-silane (Si-SCN) - which can be easily photoisomerized by UV light and subsequently modified to form functionalized patterned surfaces are investigated using Friction Force Microscopy (FFM). The applicability of FFM for the examination of chemically patterned surfaces is demonstrated and the friction contrast between modified and unmodified stripes of the patterned surface is revealed. The hierarchy of the friction coefficient of at least three different surface terminations could be identified. Through a Photo-Fries rearrangement, an acetic acid 4-(2-trichlorosilanyl-ethyl)-phenyl ester layer can form a patterned functionalized surface using lithographic techniques and post modification. FFM measurements have been utilized to detect chemical contrast on these patterned surfaces, too.

Keywords: organic surface layer, Atomic Force Microscopy (AFM), surface roughness parameters, contact angle measurement, Friction Force Microscopy (FFM), friction contrast, photosensitive organosilane surface, photoisomerization with UV light, functionalized patterned surface.

Kurzfassung

Eine neue Gruppe von Materialen, die organischen Halbleiter, wurde für neue Anwendungsbereiche entwickelt, wie zum Beispiel großflächige Beleuchtung und biegsame Bildschirme, organische Solarzellen oder moderne preiswerte elektronische Bauteile. Die Leistungsfähigkeit dieser Bauelemente ist stark abhängig von den Oberflächeneigenschaften der Grenzschicht zwischen dem organischen Halbleiter und dem Substrat. Dieser Beitrag befasst sich mit der Oberflächenuntersuchung von drei verschiedenen organischen Oberflächenschichten. Organische selbstorganisierende Silan-Multilagen, insbesondere Schichten von (Heptadecafluoro-1,1,2,2-tetrahydrodecyl) trichlorosilane (PFDTS) und 2-(4-Chlorosulfonylphenyl) ethyltrichlorosilane (CSTS), werden in organischen Dünnfilmtransistoren als Grenzschicht genutzt und können die Leistungsfähigkeit des elektronischen Bauteils stark beeinflussen. Mittels Rasterkraftmikroskopie werden charakteristische Kenngrößen der Oberflächenrauigkeit bestimmt. Aus dem Vergleich der Oberflächeneigenschaften von Schichten, die nach verschieden Methoden hergestellt wurden, ergibt sich, dass die Methode in einer Glove-Box die am geeignetsten ist. Kontaktwinkelmessungen wurden verwendet, um die chemische Änderung der Oberfläche zu untersuchen. Die zweite photoempfindliche organische Silan-Oberflächenschicht - Dünnschichten aus (4-thiocyanatomethyl) phenyltrimethoxysilane (Si-SCN) - kann mit UV-Licht photo-isomerisiert werden und anschließend zur Herstellung einer funktionalisierten strukturierten Oberfläche für die Modifikation von inorganischer Oberflächen benutzt werden. Mittels Rasterkraftmikroskopie wird die Erzielung eines Reibungskontrasts zwischen modifizierten und unmodifizierten Oberflächenabschnitten auf strukturierten Proben demonstriert. Die Hierarchie des Reibungskoeffizients von mindestens drei verschiedenen Oberflächenmodifikationen konnte ermittelt werden. Durch eine Photo-Fries-Umlagerung, die Verwendung von lithographischen Techniken und weitere Postmodifikation können auch strukturierte funktionalisierte Oberflächen aus acetic acid 4-(2-trichlorosilanyl-ethyl)-phenyl ester erzeugt werden. Durch FFM Messungen wurde an diesen Proben ebenfalls ein chemischer Kontrast erzielt.

Schlagwörter: organische Oberflächenschicht, Rasterkraftmikroskopie, Kenngrößen der Oberflächenrauigkeit, Kontaktwinkelsmessung, Reibungskraftmikroskopie, Reibungskontrast, photoempfindliche organische Silan-Oberflächenschicht, Photo-Isomerisieren mit UV-Licht, funktionalisierte strukturierte Oberfläche.

Acknowledgement

First of all, I would like to thank **Ao. Univ. Prof. Dr. Christian Teichert** and **Dipl.-Ing. Dr. mont. Gregor Hlawacek** for their patience, attentions and expert in my work. Without their strict guidance and untiring supervision, I would have not finished this work in time.
I would like to thank all current and former members of the scanning probe microscopy group, especially **Dipl.-Ing. Franz Schmied** for the final corrections, **Dipl.-Ing. Yue Hou** and **Dipl.-Ing. Thomas Klünsner** for their timely help, and **Nurdogan Gürkan** for his contact angle measurement. Also I want to thank all the people at the Institute of Physics for giving me a pleasant working atmosphere, especially **Heide Kirchberger** and **Magdalena Ottrin** for the administrative support.
This diploma thesis was performed in cooperation with the project "Interface controlled and Functionalized Organic Films" (S9702-N08 + S9707-N08) supported by Austrian Science Fund FWF National Research Network and Joaneum Research.
During this project, I would like to thank the people in Institute for Chemistry and Technology of Organic Materials in Graz University of Technology: **Ao. Univ. Prof. Mag. Dr. Wolfgang Kern**, **Dr. Gregor Trimmel** and **Dipl.-Ing. Thomas Höfler**, etc. for providing me with samples of their organic surface layers, especially **Dr. Alexander Lex** and **Dr. Thomas Grießer** for trying to answer my chemical questions at all times. And I will also thank the group of **Ao. Univ. Prof. Dr. Roland Resel** for the XRR and XPS measurements for these samples.
For giving me the opportunity to study abroad, inexhaustible supports and love, I would like to thank my parents and my big family.
Thanks to all the people who made free and powerful Gwyddion software for all SPM analyses.

Table of content

1 Introduction……..1
1.1 Motivation……1
1.2 Organic surface layers……..2
1.2.1 Organic surface layers……2
1.2.2 Chemical structure (PFDTS, CSTS)……..3
1.3 Photoreactive surface layers……3
1.3.1 Si-SCN surface layer……3
1.3.2 Ester surface layer……4

2 Experimental……6
2.1 Substrate pre-treatment……6
2.1.1 Substrates……..6
2.1.2 Surface pre-treatments (plasma etching and water dip)……6
2.2 Film preparation……...7
2.2.1 Preparation of organic surface layers (PFDTS and CSTS)……...7
2.2.1.1 Preparation under a fume hood (Method 1)……...7
2.2.1.2 Preparation in a glove box (Method 2)……..7
2.2.1.3 Evaporation of the films (Method 3)……..8
2.2.1.4 Wiping process ……..8
2.2.2 Preparation of photoreactive layers……8
2.2.2.1 Si-SCN organic surface layer……8
2.2.2.1.1 Synthesis of Si-SCN molecule……8
2.2.2.1.2 Preparation of Si-SCN layer……9
2.2.2.1.3 Illumination with UV light……..9
2.2.2.1.4 Post modification……10
2.2.2.2 Ester organic surface layer……11
2.2.2.2.1 Synthesis of ester molecules……..11
2.2.2.2.2 Preparation of ester layer……..11
2.2.2.2.3 UV illumination and post modification……11
2.3 Atomic Force Microscopy……12
2.3.1 AFM principle……..12
2.3.1.1 AFM in Contact Mode……14
2.3.1.2 AFM in Tapping Mode……14
2.3.1.3 Phase imaging……..……14
2.3.2 AFM probes……14
2.3.3 Roughness characterization……15
2.4 Friction Force Microscopy……16
2.4.1 FFM principle……16
2.4.2 FFM probes……17
2.4.3 FFM analysis……17
2.5 Contact angle measurements……..18

3 Results…………………………………………………………………………20
3.1 Investigation of substrate surfaces…………………………………………20
3.1.1 Surface pre-treatment by plasma etching………………………………20
3.3.2 Two different substrate types…………………………………………...21
3.3.2.1 Si-SCN surface layer unilluminated on the Infineon type substrate……………………………………………………………..21
3.3.2.2 Si-SCN surface layer unilluminated on the Sigert type substrate……………………………………………………………..22
3.2 Organic surface layers (PFDTS, CSTS)……………………………………23
3.2.1 Surface morphology without wiping process………………………...23
3.2.1.1 PFDTS surface layer……………………………………………..23
3.2.1.2 CSTS surface layer………………………………………………25
3.2.2 Comparison of 3 different methods after the wiping process………..25
3.2.2.1 PFDTS surface layer……………………………………………..26
3.2.2.2 CSTS surface layer………………………………………………28
3.2.2.3 Contact angle measurements of PFDTS and CSTS surface layers……………………………………………………………..29
3.3 Photoreactive thin layers……………………………………………..….29
3.3.1 Surface morphology for different deposition, concentration, and time…………………………………………………………………..29
3.3.1.1 The lying sample…………………………………………………30
3.3.1.2 The standing sample……………………………………………..31
3.3.2 Surface morphology after post modification…………………………32
3.3.3 Friction force contrast patterns after UV illumination through different stripe masks……………………………………………………………..34
3.3.4 Friction force contrast patterns after post modification through different stripe masks………………………………………………36
3.3.4.1 Modification with PA after UV illumination……………………36
3.3.4.2 Modification with FA after UV illumination……………………37
3.3.5 Friction force contrast after applying two crossed masks…………..39
3.3.6 Friction force contrast of an ester surface layer……………………..41

4 Discussion and Conclusions……………………………………………………..43
4.1 Influence of the plasma etching process on the substrate roughness………..43
4.2 Influence of the substrate types on Si-SCN thin surface layer morphology…43
4.3 Influence of the preparation processes on the morphology of the surface layer……………………………………………………………………44
4.4 Influence of the deposition conditions on Si-SCN surface layer morphology………………………………………..…………………45
4.5 Influence of the Si-SCN layer preparation process on surface roughness…..46
4.6 Influence of the post modifications on Si-SCN surface layer morphology….47
4.7 Identification of two surface terminations on the stripe pattern by FFM……47
4.8 Identification of four surface terminations on the patterned surface by FFM…………………..………………………………………………49

4.9 Influence of termination polarity and stiffness on friction force……………50
4.10 Final discussion of the applicability of FFM measurements……………….51

5 Summary and Outlook……………………………………………………54

6 References……………………………………………………………56

7 List of Abbreviations…………………………………………………..58

8 Appendixes………………………..59

1 Introduction

1.1 Motivation

Now, at the beginning of the 21st century we are facing a new electronics revolution that has become possible due to the development and understanding of a new class of materials, commonly known as organic semiconductors. The enormous progress in this field has been driven by the expectation to realize new applications, such as large area, flexible light sources and displays, low-cost printed integrated circuits or plastic solar cells from these materials [1].

Modern low cost devices are increasingly based on organic semiconductors. This important class of materials is expected to serve well-priced thin film transistors and optical components such as light emitting diodes [2]. The device performance is significantly influenced by the interface between the organic semiconductor and the inorganic electric components and its surface morphology. An important intermediate step towards technological application is the possibility to control the growth behavior of active organic materials in terms of orientation and structure on short length scales [2].

Here, Atomic Force Microscopy (AFM) based techniques are applied to study the morphology and physical properties of organic thin films. In particular, Friction Force Microscopy (FFM) has been adapted to reveal a materials contrast in patterned photoreactive layers. The first organic thin films - we focus on in this investigation - are commercially available organosilane self-assembled oligolayers, which are of great interest for various applications including the engineering of surface properties over a wide range as well as immobilization of catalysts, biomolecules and in nanotechnology. They can be applied as adhesion promoters between organic and inorganic compounds for control of the wettability, surface polarity, and chemical reactivity [4]. Moreover, these layers have been applied as interfacial layers in Organic Thin Film Transistors (OTFTs), strongly impacting the final device performance [5]. Here, AFM with assistance of Contact Angle (CA) Measurements is used to analyze the surface properties on the nanometer and micrometer scale to optimize the sample preparation.

The second type of organic thin films under investigation is novel photosensitive organosilane surface layer, which can be easily isomerized by UV light and subsequently modified to form a patterned surface with different functionalized surface terminations. This patterned functionalized surface is a promising substrate for applications in modern immobilization techniques and for the structured modification of inorganic surfaces [6] and can also be applied to the fabrication and integration of Organic Light Emitting Diodes (OLEDs) and OTFTs. Using FFM, the chemical contrast between modified and unmodified regions of the patterned surface and the hierarchical order on the surface can be revealed and distinguished [3].

The third class of organic thin films investigated here is photosensitive layer, which undergoes a Photo-Fries rearrangement with UV light. The generated hydroxyketone

group changes the refractive index and the surface polarity. By choosing different acid chloride, the surface properties can be tuned in a wide range. In combination with further post exposure modification reactions and lithographic techniques, patterned functionalized surfaces can be obtained [7].
In this thesis, first, an introduction to the chemical preparation of these three organic thin surface layers and the experimental setup will be given. Then, the morphological results as well as the data of the FFM investigations of these films will be presented. The quantitative roughness analysis and a systematic discussion of FFM results will follow. In the end, an outlook to future FFM investigations will be given.

1.2 Organic surface layers

1.2.1 Organic surface layers

The organosilane-based thin layers under investigation are thin siloxane layers with different functional end groups on silicon oxide surfaces. The structure of this layer is similar to the one of self-assembled multilayers. This self-assembling surfactant molecule monolayer is well-organized, and consists of three parts: The end of the molecule facing the substrate is called head group. It is chemisorbed on the surface due to a strong interaction (covalent bond) with the substrate [8]. The second molecular part (spacer) is an organic moiety, which is responsible for the self-organization of the layer. In most cases it is a long alkyl chain. The energies associated with its interchain van der Waals interactions depend on both the chain length and the packing density [9]. The third part on the other end of the molecule – called tail group - is the functional group, which controls the chemical properties of the film surface. A scheme of a self-assembled monolayer (SAM) is shown in Figure 1.

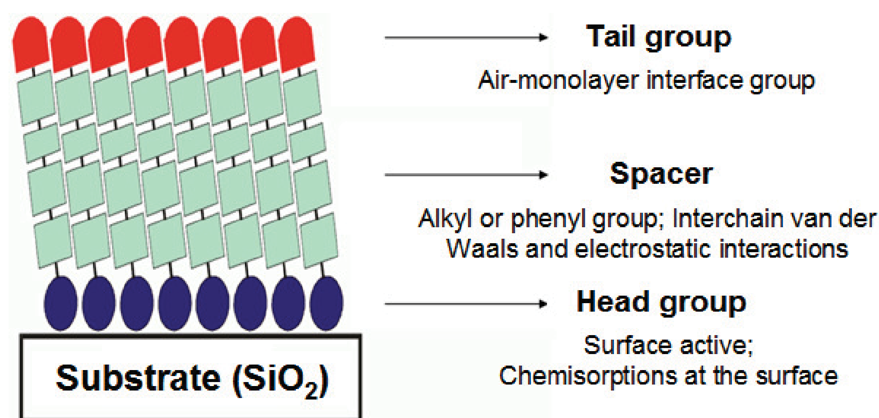

Figure 1: A schematic view of the structure and the forces in a SAM (Head group: covalent bond to substrate (SiO_2); Spacer: controls the molecule arrangement of the surface layer; Tail group (functional group): determines chemical properties of the surface layer).

1.2.2 Chemical structure (PFDTS, CSTS)

In this context, we focus on AFM studies of two self-assembled monolayer systems, whose molecules are shown in Figure 2: thin layers of (Heptadecafluoro-1,1,2,2-tetrahydrodecyl) trichlorosilane (PFDTS) and 2-(4-Chlorosulfonyl- phenyl) ethyltrichlorosilane (CSTS). PFDTS consists of a silane head group, a long alkyl chain spacer and a fluorid tail group. The molecule's length is 1.4 nm. The other thin layer, CSTS, consists of a silane head group, a long benzyl chain spacer and sulfonic acid chloride tail group. The molecule's length is 0.9 nm.

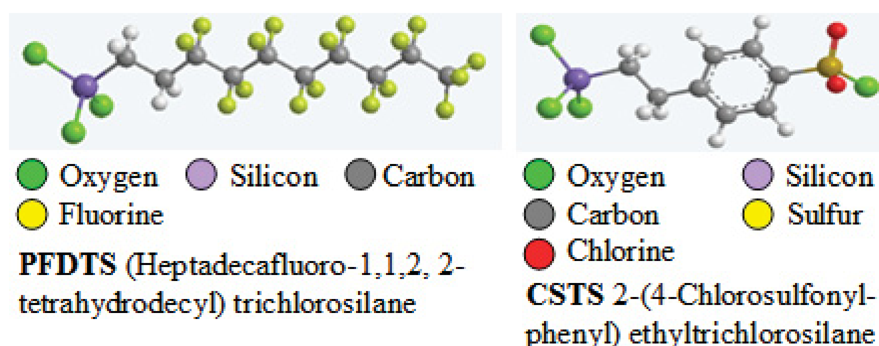

Figure 2: Chemical Structure of PFDTS and CSTS molecule system.

The thickness of these surface layers was extracted from best curve fits of a grazing incidence X-ray reflection (XRR) measurement performed within the group of Roland Resel, Institute of Solid State Physics at Graz University of Technology. According to the X-ray results, the CSTS film fabricated under inert gas dry conditions has a thickness of 2.4 nm which corresponds to approximately 2.5 monolayer equivalent. Also, the thickness of the PFDTS film is much larger than its molecular length. These surface layers are therefore composed of several ill defined layers and do not correspond to a single monolayer. Using AFM measurements, the morphology of these surface layers (layer by layer growth or head-to-head combination clusters) will be discussed in chapter 3.2.

1.3 Photoreactive surface layers

1.3.1 Si-SCN surface layer

The Si-SCN surface layer is composed of a novel photosensitive molecule (4-thiocyanatomethyl) phenyltrimethoxysilane (Si-SCN) [6], which is produced by the Institute of Chemistry and Technology of Organic Materials of Graz University of Technology.

This thin layer of bifunctional organosilanes contains a thrimethoxysilyl moiety and a benzyl thiocyanate moiety. The thrimethoxysilyl moiety, as the anchoring group to

substrates, binds to surface hydroxyl groups of inorganic oxides. The photoreactive benzyl thiocyanate moiety, which is separated by an aryl spacer from the anchoring group, determines the final properties of the surface layer [6].
The photosensitive benzyl thiocyanate group can be used to modify the oxidized silicon surface. Upon exposure to UV light, the thiocyanate (SCN) undergoes a photoisomerization to the corresponding isothiocyanate (NCS), which is accompanied by a drastic change in the physical properties and the chemical reactivity. Subsequently, the isothiocyanate (NCS) can be modified selectively with propylamine to the corresponding thiourea compound (propylamine - PA). The isomerization and modification scheme is shown in Figure 3.

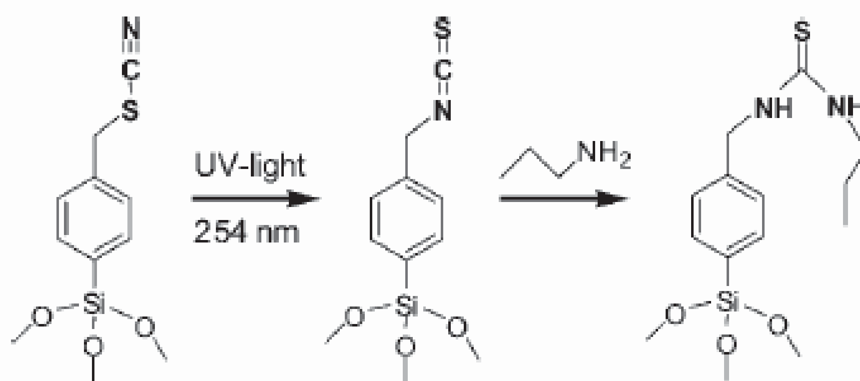

Figure 3: Photoisomerization and post modification of benzyl thiocyanate (from [6]).

1.3.2 Ester surface layer

This photosensitive surface layer is a novel organic functional trichlorosilane layer bearing the acetic acid 4-(2-trichlorosilanyl-ethyl)-phenyl ester, which is self-assembled on silicon oxide surfaces [6]. This ester molecule was also synthesized by the Institute of Chemistry and Technology of Organic Materials of Graz University of Technology.
Upon irradiation with UV light, this ester undergoes a Photo-Fries rearrangement [7], which is shown in Figure 4 and can be depicted as follows: under illumination with UV-light, the scission of the C-O bonds leads to the cleavage of the aromatic ester into the acyl and the phenoxyl radical. The photogenerated radicals can recombine to the o- or p-cyclohexadienone derivatives as the "cage product". The tautomerism yields the corresponding hydroxyketones. The free phenol formed is an "escape product" and decarboxylation can occur as a competing reaction [10]. The Photo-Fries reaction represents a versatile tool for tuning the surface properties, optical patterning, and polymer functionalization [7].

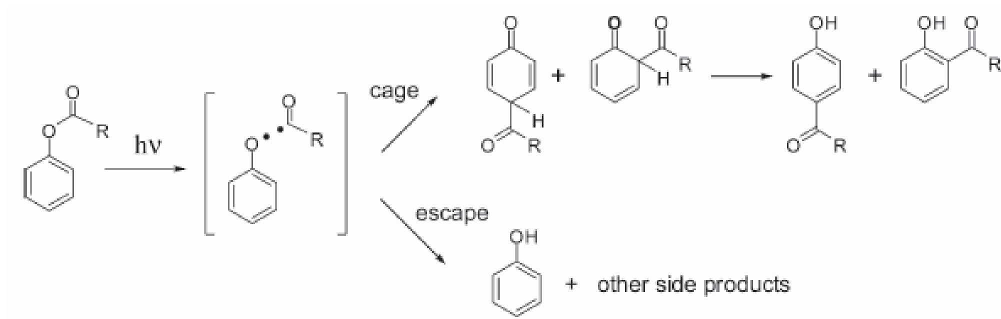

Figure 4: Reaction mechanism of the Photo-Fries rearrangement (from [7]).

After the Photo-Fries rearrangement, the aromatic hydroxyketone group enhances the chemical reactivity as well as the refractive index, surface tension, and surface polarity of the illuminated areas. It can be employed as an excellent precursor for a selective post modification with different carboxylic acid chlorides (e.g.: perfluorobutyryl chloride) to form new ester groups. Using a lithographic process and choosing different acid chlorides, functionalized polymer surface can be obtained and the surface properties of such films can be tuned in a wide range [7].

2 Experimental

General:
All chemicals were purchased from commercial sources and used without further purification. All organic thin films investigated have been prepared by the Institute for Chemistry and Technology of Organic Materials in Graz University of Technology and the Chair for Synthesis of Special and Functional Polymers at the University of Leoben. All chemical experiments were carried out under Argon atmosphere using Schlenk techniques [13].

Hazard warnings:
Because UV irradiation causes severe eye and skin burns, precautions (UV protective goggles, gloves) must be taken. In the following description of pre-treatments, synthesis and post modification reaction of the organic thin surface layers, hazardous chemicals and solvents are used (methanol, piranha solution, PA, acid chlorides, et al.). In addition, Piranha solution is extremely corrosive and explosive, and its preparation is highly exothermic (up to 120°C). Therefore, reactions must be carried out in a fume hood and protective gloves and goggles are absolutely necessary [6].

2.1 Sample pre-treatment

2.1.1 Substrates

Two kinds of different substrates for the organic surface layers were used: one was a single-side-polished p-type-doped (B) silicon wafer with a native silicon oxide (resistivity 9-18 Ωcm) from Infineon Technologies Austria AG, which is used for Fourier Transform Infrared (FTIR) Spectroscopy measurements. The other was a single-side-polished silicon wafer (n-type-doped (N/AS), resistivity < 0.003 Ωcm) with a thermally grown 165 nm thick silicon oxide layer from Sigert Consulting e.K. as substrate, which is used for X-ray Photoelectron Spectroscopy (XPS) and XRR measurements [4]. For the AFM measurements both the "Infineon type" and "Sigert type" substrates were cut into 1×1 cm^2 pieces.

2.1.2 Surface pre-treatments (plasma etching and water dip)

The substrate wafers have to be pretreated to obtain a good attachment between the substrate surface and the growing thin layer. For this purpose, a plasma etching cleaning step – which was performed in a home build plasma etch machine at the Department of Solid State Physics of the Graz University of Technology [14] - was used to obtain a hydrophilic surface with a high concentration of surface hydroxyl

groups [11]. The substrate was etched with the oxygen plasma for 30 seconds, which decreases the CA of water from 70°-90° to about 40°, and subsequently dipped into deionized water (18 MΩcm, Milli-Q) for 2 minutes, which leads to a reproducible hydrophilic surface with a CA of less than 10°. Afterwards, the samples were dried with CO_2 until no traces of water drops were visible [4]. The surface change by these pretreatments of plasma etching and a water dip is demonstrated by representative CA photographs in Figure 5.

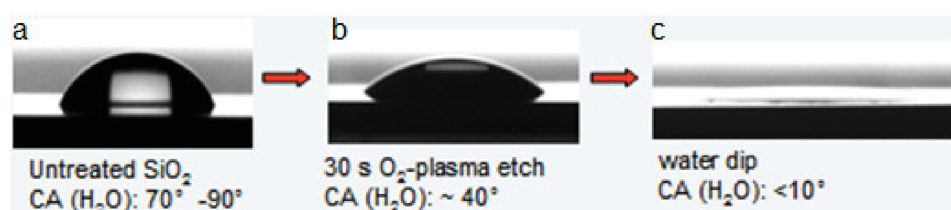

Figure 5: CA photographs of pretreatment of the SiO_2 surface a) untreated surface with water CA 70°-90°, b) after plasma etching the water CA is changed to 40°, c) the water CA decreases less than 10° by using a water dip step (from [14]).

2.2 Film preparation

2.2.1 Preparation of organic surface layers (PFDTS and CSTS)

There have been three different layer preparation methods [4] used for (Heptadecafluoro-1,1,2,2-tetrahydrodecyl) trichlorosilane (PFDTS) and 2-(4-Chlorosulfonylphenyl) ethyltrichlorosilane (CSTS) organic surface layers, which will be discussed in detail as follows:

2.2.1.1 Preparation under a fume hood (Method 1)

The substrates were evacuated for 10 minutes and immersed in a 0.1 vol% solution of trichlorosilane in High Performance Liquid Chromatography Grade (HPLC-grade) toluene under a fume hood at room temperature for 16 hours. Afterwards, the substrates were sonicated for 2 minutes in fresh toluene, dried in a CO_2 stream, selectively wiped off with a tissue drenched in toluene, sonicated again for 2 minutes in toluene and dried with CO_2. All the reactions were carried out under the fume hood.

2.2.1.2 Preparation in a glove box (Method 2)

After evacuation (10 min) and immersion in a 0.1vol% solution of trichlorosilane in distilled toluene in a nitrogen glove box at room temperature for 16 hours, the substrates were sonicated for 2 minutes in fresh toluene, dried in a CO_2 stream, selectively wiped off with a tissue drenched in toluene, sonicated again for 2 minutes in toluene and dried with CO_2. All the reactions were carried out in a glove box.

2.2.1.3 Evaporation of the films (Method 3)

This is not a wet chemical method as Methods 1 and 2. All the PFDTS and CSTS molecules were evaporated and formed on the substrate in a closed glass chamber. The pretreated substrate and a small amount of trichlorosilane in a vial were put in a closed glass chamber and the whole system was kept at 120°C in a clean oven for 16 hours. Afterwards, the substrates were selectively wiped off with a tissue drenched in toluene, sonicated in toluene for 2 minutes, and dried with CO_2.

2.2.1.4 Wiping process

In order to obtain a smoother surface layer after these chemical preparations, a wiping step was applied [12], which proceeded by tissue to wipe off the excessive silane molecules.

2.2.2 Preparation of photoreactive layers

Two organic photosensitive molecules, namely Si-SCN and acetic acid 4-(2-trichlorosilanyl-ethyl)-phenyl ester are used here. Irradiation with UV light and post modification are carried out to obtain patterned functionalized layers.

2.2.2.1 Si-SCN organic surface layer

2.2.2.1.1 Synthesis of Si-SCN molecule

The photosensitive molecule Si-SCN was synthesized by a straight-forward one-step reaction as depicted in Figure 6. (4-(chloromethyl) phenyl) trimethoxysilane and ammonium thiocyanate were refluxed in anhydrous methanol for 48–72 hours in a flask shaded by aluminum foil, which is used to exclude the light to avoid undesirable photoreactions [6].

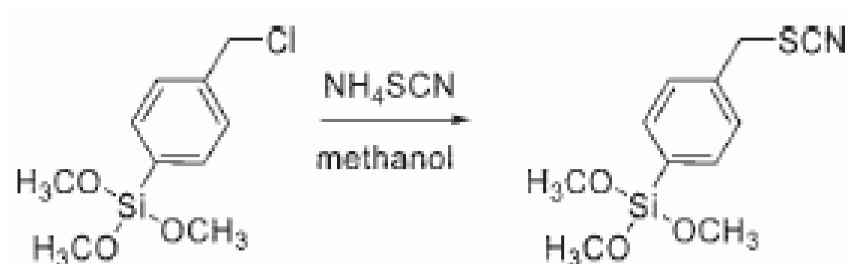

Figure 6: Synthesis of the Si-SCN molecule (from [6]).

2.2.2.1.2 Preparation of Si-SCN layer

After the pre-treatments of plasma etching and the deionized water dip, the clean substrate wafers were immersed into a 0.1 vol% or 0.01 vol% solution of Si-SCN in

HPLC-grade toluene at room temperature under ambient conditions for different time intervals. Afterwards, they were transferred to cleaned glasses with fresh toluene, sonicated for 2 min, rinsed with toluene, dried with CO_2, and annealed for 30 minutes at 100 °C in vacuum [6].

The Si-SCN layer thickness was determined by XRR measurements within collaboration with the Graz University of Technology. The XRR measurements revealed a Si-SCN layer thickness of 6.3 nm. This result indicated that this is not a monolayer but an oligolayer, which is equivalent to 5-6 individual layers (assuming upright standing molecules). The increased thickness is attributed to cross-linking of the trimethoxysilane groups in the presence of water, which results in multilayer formation [15]. Using shorter immersion times and ultra dry conditions, thinner films can be produced. However, because of poor reproducibility and exhibited inhomogeneous surface layer due to island formation, only the 6 nm "thick" oligolayers, which are well-reproducible and represent a smooth surface [6], were chosen for further processing and investigation.

2.2.2.1.3 Illumination with UV light

The irradiation experiments were carried out under argon gas to avoid photo-oxidation. As UV light sources an ozone-free mercury low-pressure UV lamp (Heraeus Noblelight; 256 nm) or an UV lamp (model UVLMS-38 3 from UVP, Upland, CA) with 254 nm wavelength were used. Using spectroradiometer measurements, the light intensity at the sample surface was determined to be 1.35 $mWcm^{-2}$ and 0.18 $mWcm^{-2}$, respectively [6].

In order to obtain patterns of irradiated and nonirradiated areas, the illumination was performed through contact masks (Cr pattern on quartz, Austria Microsystems, Unterpremstaetten, Austria). Figure 7 represents one of these masks applied here. Their thickness is about 2.5 mm (length: 26 mm; breadth: 20 mm). Three different contact masks with different equidistant lines and spaces of 3 µm, 5 µm and 10 µm have been used.

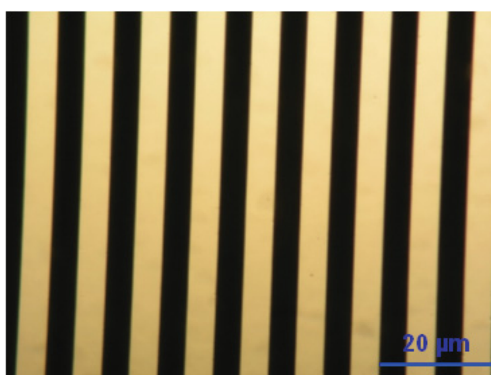

Figure 7: Optical micrograph of the contact mask having 5 µm stripes and 5 µm spacing used in UV illumination experiments.

When such a mask is placed directly on the surface layer, only the uncovered photoreactive SCN group can undergo an isomerization reaction to the corresponding NCS group during the illumination with UV light. After this irradiation step, a patterned structure, which is composed of alternating stripes with either Si-SCN or Si-NCS surface terminations can be found on this organic surface layer.

2.2.2.1.4 Post modification

After UV illumination of the SCN surface, post modification reactions with different reactants (PA or 2,2,2-trifluoroethylamine) were performed by exposing the isomerized layers to vapors of these amines [6]. On the sample's surface, only the NCS surface termination can be modified to resulting surface terminations, which are called correspondingly PA and fluorinated amine (FA) terminations. The details of these isomerization and post modification processes of this Si-SCN organic surface layer are shown in Figure 8.

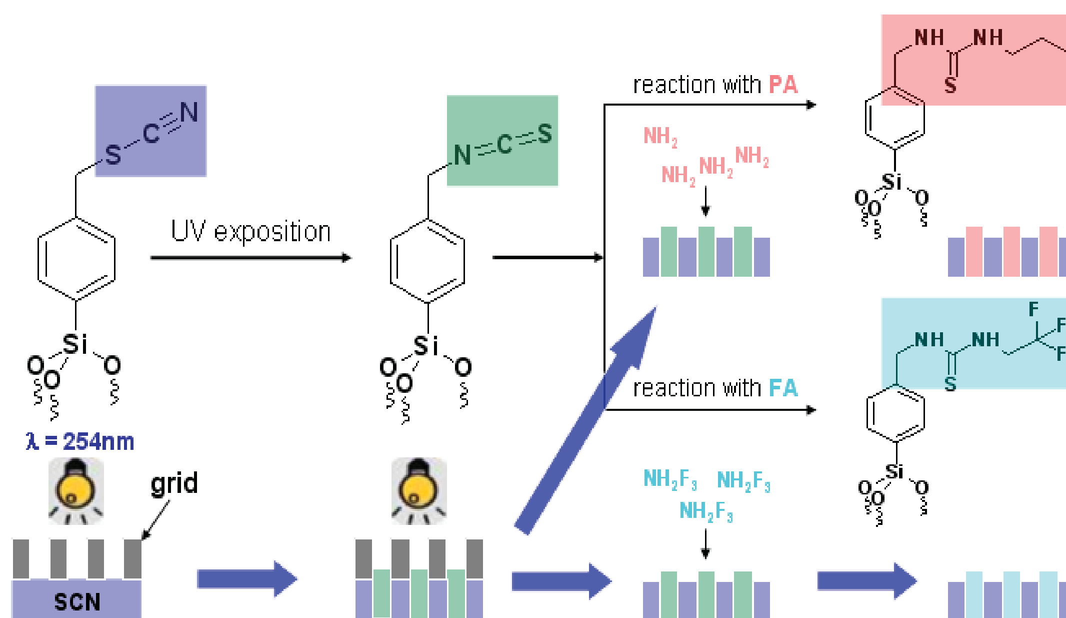

Figure 8: Si-SCN thin film isomerization and post modification processes with either propylamine (PA) or fluorinated amine (FA).

These photoreaction and post modification reactions with gaseous amines are monitored by FTIR spectroscopy and XPS, which are also in collaboration with the Graz University of Technology. Kinetic investigation of liquid films of Si-SCN by FTIR spectroscopy shows that the SCN is almost quantitatively consumed during illumination under inert atmosphere, but only 25-30% of NCS is formed because of side reactions. However, almost all the NCS is sufficient (approximately 100%) for post modification reaction with gaseous amines to the PA.

During the XPS measurement, the post modification with PA results only in a slight change in the XPS spectra because of the low yield of the photoisomerization (approximately 30%). In order to obtain a better illustration of the post modification,

this fluorinated amine 2,2,2-trifluoroethylamine was chosen as another reactant for post modification because fluorine can be easily detected by XPS [6].

2.2.2.2 Ester organic surface layer

2.2.2.2.1 Synthesis of ester molecules

The organic functional molecule acetic acid 4-(2-trichlorosilanyl-ethyl)-phenyl ester was synthesized in a one-step reaction as illustrated in Figure 9. Using a catalytic amount of H_2PtCl_6 as hydrosilation catalyst, trichlorosilane was reacted with acetic acid, 4-vinylphenyl ester in anhydrous Tetrahydrofuran (THF). In addition, all the reactions must exclude light to avoid undesirable photoreactions. Because of the hydrolytic sensitivity of the trichlorosilyl group, the synthesis must proceed under dry conditions [13].

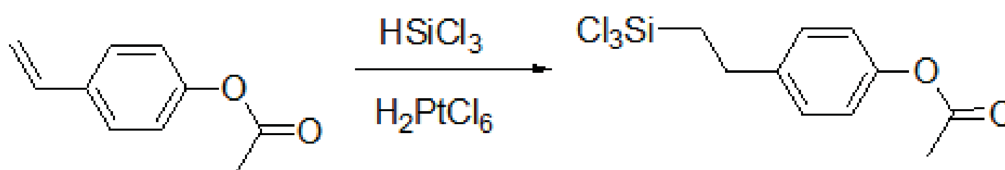

Figure 9: Synthesis of acetic acid 4-(2-trichlorosilanyl-ethyl)-phenyl ester molecule (from [13]).

2.2.2.2.2 Preparation of ester layer

After the surface pre-treatments, the clean SiO_2 substrate wafers were immersed into a 0.2% solution of acetic acid 4-(2-trichlorosilanyl-ethyl)-phenyl ester in pure toluene at room temperature for 16 hours under ultra dry inert gas condition (N_2 glove box) or under ambient atmosphere using HPLC-grade toluene, subsequently rinsed with fresh toluene, dried with CO_2 and annealed at 110°C for 30 min in vacuum [13].

2.2.2.2.3 UV illumination and post modification

The UV irradiation was again through contact masks described in chapter 2.2.2.1.3. Under illumination with UV light, only uncovered photoreactive esters can undergo the Photo-Fries rearrangement to form a hydroxyketone. After UV illumination of the ester surface, the post modification reactions were carried out as follows: The ester layer sample was immersed into a solution of perfluorobutyryl chloride and of pyridine as acid scavenger, after 2 hours rinsed with CH_2Cl_2 and dried in a stream of CO_2. In this post modification step, only the area with the hydroxyketone surface termination can be modified with perfluorobutyryl chloride to a perfluorobutyryl surface termination [13]. The photoreaction and a subsequent post-modification process are shown in Figure 10. After this post modification, a patterned functional

surface, which consists of alternating stripes of the unmodified (acetoxy group) and the modified (perfluorobutyryl group) surface termination, can be found on this ester surface layer.

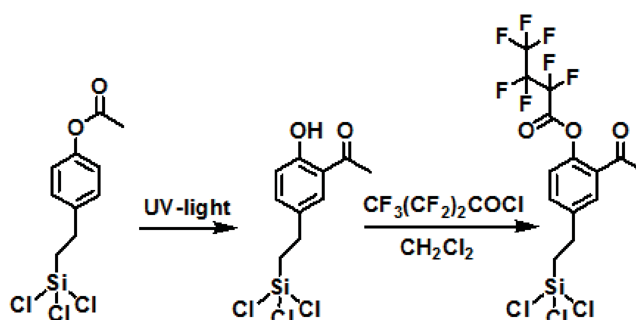

Figure 10: UV illumination and post modification with perfluorobutyryl chloride of the ester surface layer (from [13]).

2.3 Atomic Force Microscopy

2.3.1 AFM principle

Atomic force microscopy has been developed by Binnig and colleagues in 1986 [16]. Now, AFM has become also a versatile modern technique of immense applications in such areas as thin films and colloid science [17]. It operates on conducting and non-conducting surfaces as well. The imaging method by “feeling” rather than “looking” can produce detailed, laterally resolved information, not just of the surface topography but also of its materials characteristics, soft of hard, springy or compliant, sticky or slippery on the specimen surface [16].
Figure 11 illustrates the main features of an AFM. In AFM, a tip located on the end of a cantilever scans the sample surface using piezoelectric scanners. In our approach, a scanning sample design is used, thus the sample is scanned underneath a fixed probe. The probe tip senses surface forces arising from various interactions (van der Waals, electrostatic, hydration, etc.) between the tip and the sample surface. The changes in the tip-sample interaction are often monitored using an optical detection system, in which the deflection of the cantilever is detected by the reflection of a laser beam, which is reflected onto a position-sensitive photodiode (PSD). Usually, AFM is operated under a constant-force mode and the z-motion of the piezoelectric scanner maintains a fixed bending of the cantilever. AFM images are generated through a feedback loop between the detection system and piezoelectric scanner.

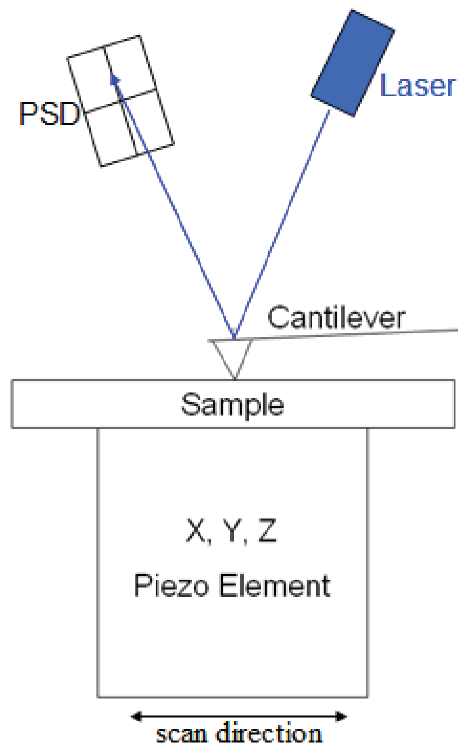

Figure 11: Schematic representation of the AFM principle.

The AFM results were obtained with a Digital Instruments (DI) Nanoscope Multimode IIIa atomic force microscope (see Figure 12) equipped with a tube scanner. Its maximum lateral scan size is 125 μm×125 μm and the maximum travel distance of the z-piezo is 5 μm. The DI software version V613r1 is used.

Figure 12: DI Nanoscope Multimode IIIa Scanning Microscope.

As processing of the obtained AFM images, first order flattening was used to eliminate scanning artefacts. Then, a third order plane fit was used in all topography images to compensate for surface bowing due to the use of a tube scanner. Three imaging modes, contact mode, intermittent contact mode (tapping mode), and non-contact mode, can be used to produce topographic images of sample surfaces.

2.3.1.1 AFM in Contact Mode

In contact mode, the AFM tip is brought into direct contact with the sample and is then dragged cross the surface. When the tip nearly touches the surface, attractive forces dominate between the tip and surface and make the tip adsorb on the surface. The larger the cantilever is bent, the higher is the applied force. To minimize the imaging force used to scan the sample, low spring constant ($k < 1$ N/m) cantilever are normally used. However, for soft sample surfaces deformation and damage often occurs during contact mode imaging in air because significant forces must be applied to overcome the effects of surface contaminations (e.g.: adsorbed moisture). With a significant normal force, the lateral forces created by the dragging motion of the probe tip across the sample can result in high contact stresses in a small contact area, which can damage either the sample or the tip, or both.

2.3.1.2 AFM in Tapping Mode

To reduce or eliminate the lateral forces associated with contact mode, the cantilever can be oscillated near its first bending mode resonance frequency. The scanned tip touches the surface discontinuously at constant force and can sensitively produce the surface morphological image through the oscillating contacts between the tip and the surface. The tapping mode (also called intermittent-contact mode) allows characterizing the surface morphology in the absence of lateral forces that might otherwise alter the tip or surface morphology and has the same resolution as contact mode. The disadvantage of tapping mode relative to contact mode is the slightly slower scanning speed. Here, all topography images - devoted for comprehensive surface roughness analysis (see chapter 2.3.3) – have been recorded in tapping mode.

2.3.1.3 Phase imaging

The changes of phase angle of the cantilever oscillation can be recorded in tapping mode to produce a second image, the so called phase image. The image often provides significantly more contrast than the topographic image and has been shown to be sensitive to materials properties, such as stiffness, viscoelasticity, and chemical composition. A reasonable level of contrast in a phase image is primarily dependent on the measurement of at least two components in the sample with sufficiently different elastic properties [16].

2.3.2 AFM probes

The AFM probes used for tapping mode measurements are Pointprobe®plus PPP-NCHR probes made of highly doped n^+- single crystal silicon (resistivity: 0.01-0.02 Ωm) produced by Nanosensors™ for non-contact (tapping mode) with a rectangular cantilever with trapezoidal cross section (length: 125 µm; thickness: 4 µm; width: 30 µm), which has a typical resonance frequency of 300 kHz and a force constant of 40 nN/nm.

The standard Pointprobe® tip is shaped like a polygon based pyramid. The cantilever has an Al-coating on its back side for good reflection of the laser beam. Its macroscopic half cone angle is 20° to 25° viewed along the cantilever axis, 25° to 30° when looking from the side and virtually zero at the tip end. The Pointprobe® tip is 10-15 μm high and shows a tip radius of typically better than 10 nm (see Figure 13).

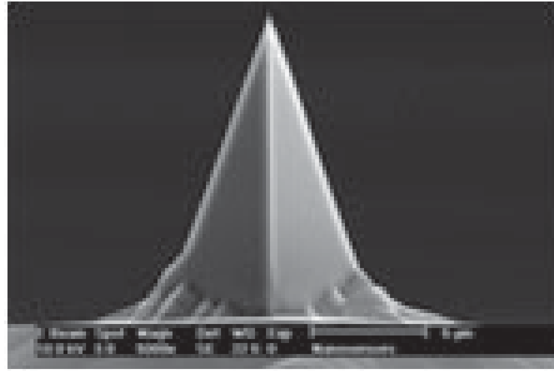

Figure 13: Pointprobe®plus PPP-NCHR Tapping Mode AFM tip (from [18]).

2.3.3 Roughness characterization

For surface roughness characterization, the root-mean-square (rms) roughness σ, the lateral correlation length ξ, and the roughness exponent α were calculated from the AFM image data by using the height-height correlation function (HHCF). All parameters were calculated by analyzing at least three independent 5 μm×5 μm images. The meaning of these constants is as follows [19]:

The rms roughness σ or the interface width describes the fluctuation of surface heights around an average surface height, thus it is sufficient to characterize vertical surface roughness for most purposes. Different rough surfaces may have the same rms roughness σ but different frequencies of the lateral height fluctuations. Therefore, it is necessary to use additional parameters to describe the surface in more details.

The correlation length ξ obtained by analyzing the height-height correlation function defines a representative lateral dimension of a rough surface, across which the height levels are correlated. ξ is usually a measure for the smallest feature size which is significantly smaller than the average lateral size of the surface features.

The roughness exponent (or Hurst parameter) α describes how jagged the surface is. The smaller α is, the more jagged the surface becomes in a qualitative picture. Typical values of α are between 0.5 (exponential decay of the HHCF) and 1 (Gaussian HHCF).

These three parameters are independent from each other and completely characterize a random rough self-affine surface [19].

2.4 Friction Force Microscopy

2.4.1 FFM principle

For Friction Force Microscopy (FFM) which is also called Lateral Force Microscopy (LFM), the fast scan direction is set perpendicular to the long axis of the cantilever. In addition to the deflection signal normally recorded in contact mode, also the horizontal deflection of the laser beam on the four-quadrant PSD is recorded (see Figure 14). The latter is a result of friction between the tip and sample surface which leads to a twisting of the cantilever. Due to the sensitivity of the friction force on chemical changes on the surface, this method is also called Chemical Force Microscopy (CFM) [20]. Here, this fact is used to differentiate between different tail groups of the film forming molecules. In principle, the FFM signal is independent of the surface morphology.

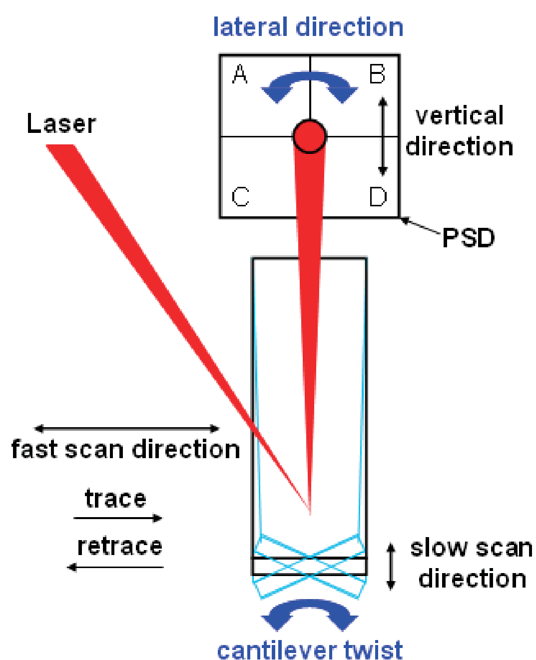

Figure 14: Scanning and Detection with FFM.

During the FFM measurement, both topography and friction force data are record simultaneously: The topographical image shows surface morphological information (z-scale is nm) obtained from the vertical deflection signal. At the same time, two friction images (trace and retrace) are recorded. In general, FFM measurements are done in constant force mode. For quantitative measurements of the friction force, a full stiffness calibration of the cantilever's mechanical properties (force constant, stiffness) is necessary. However, for obtaining only a qualitative friction contrast, this is not required. Therefore, the presented friction force images have z-scale in Volts.
A first order plane fit was used in all topography images to correct for the scanner

bow of the tube scanner due to the large image size. This procedure has not been applied to the FFM images.

2.4.2 FFM probes

The FFM probes used are specially designed Pointprobe®plus PPP-LFMR cantilevers made of highly doped n^+- single crystal silicon (resistivity: 0.01-0.02 Ωm) produced by Nanosensors^{TM}. These contact mode probes have a rectangular cantilever with a trapezoidal cross section (length: 225 µm; thickness: 1 µm; width: 48 µm) and a typically force constant of 0.2 nN/nm. The shape of this standard FFM tip is equal to normal AFM tips (see Figure 13).

2.4.3 FFM analysis

When the FFM probe scans a very flat surface, the lateral deflection of the cantilever is mainly caused by the friction between tip and surface. However, if the surface is not perfectly flat, the cantilever torsion will also be influenced by the surface morphology. Figure 15 shows that in both scan directions (trace and retrace) a real FFM signal (red signal) due to a change in friction is opposite for trace and retrace whereas a FFM signal resulting from surface morphology (green signal, coming from a steep slope) is unchanged for both directions.

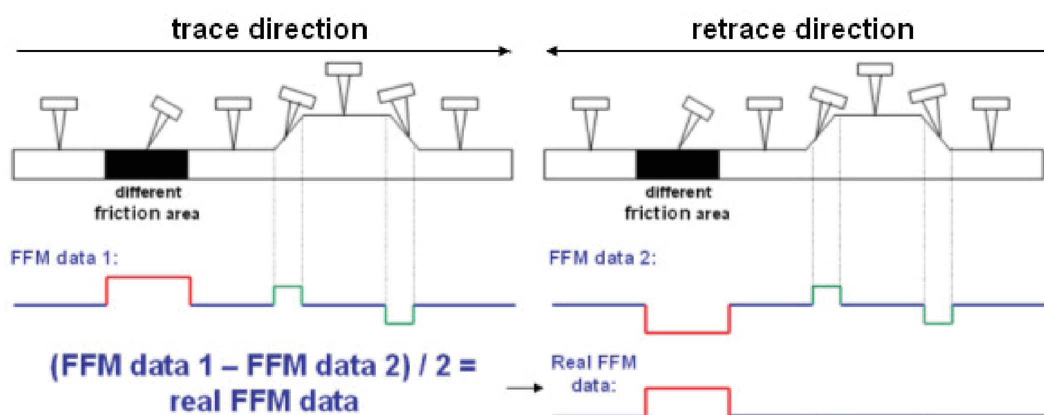

Figure 15: Lateral deflection of the cantilever from the influence of the friction (red) and topographical undulation (green).

Using the simple arithmetic subtraction operation: real FFM = (trace FFM data – retrace FFM data) / 2, the topographic effects can be removed from the final FFM image. Figure 16 shows together with the topography image (A), the FFM image recorded in trace (C) and retrace (D) direction and the calculated FFM image (B) through the subtraction operation. The real friction image calculated shows the real friction contrast on the surface without artifacts induced by surface topographical changes.

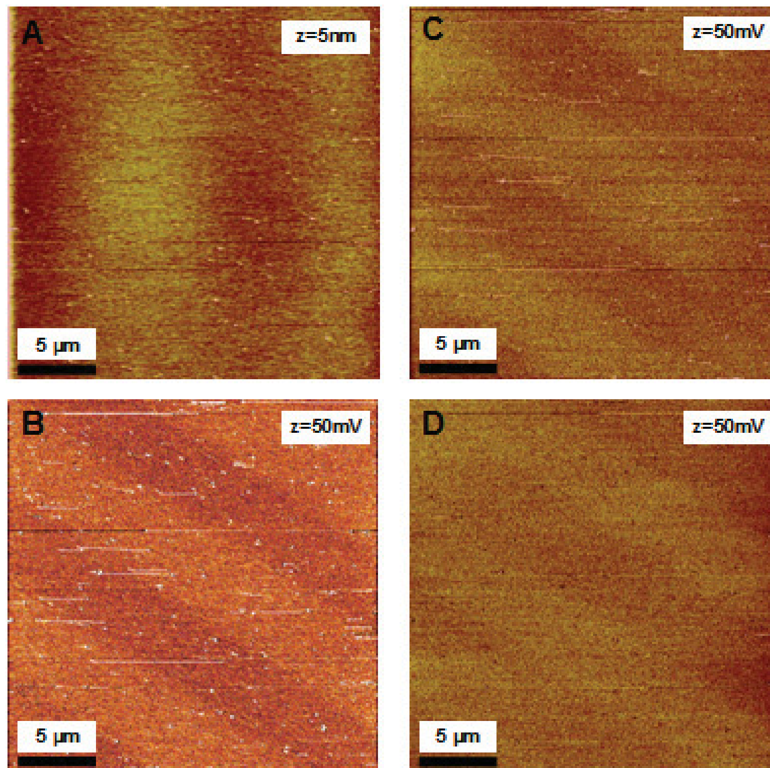

Figure 16: A: 25 µm×25 µm topography image of illuminated Si-SCN surface after modification with FA using a 5 µm wide mask, B: real friction image which is formed by the subtraction operation (trace FFM data – retrace FFM data) / 2, C: friction image in the trace scan direction, D: friction image in the retrace scan direction.

It is important to understand that Figure 15 represents an idealized situation and that in real measurements topographic effects might not be removed completely [21]. As the surface roughness will also influence the obtained friction signal [22], a comprehensive study of the surface roughness has to accompany all FFM investigations.

2.5 Contact angle measurements

CA measurement is a simple-to-adopt method for surface analysis related to surface free energy or interfacial tension (IFT). It should be noted here that both terms describe the same phenomenon and can be exchanged. When a droplet of liquid rests on the surface of a solid, the shape of the droplet is determined by the balance of the interfacial liquid/vapor/solid forces, as descried by the Young's equation. If a liquid with well-known properties is used, the resulting CA can be used to calculate the IFT and consequently identify the nature of the solid. This technique is extremely sensitive to chemical changes of the surface [23].

The CA measurements in this work were performed using a KRÜSS DSA100 M (see Figure 17), which use a piezo element to create pico-liter size droplets (min. drop size

is 100pL) and video based analyzing. The minimal achievable droplet diameter of approximately 80 µm is in the same order of magnitude as the typical image sizes in AFM measurements.

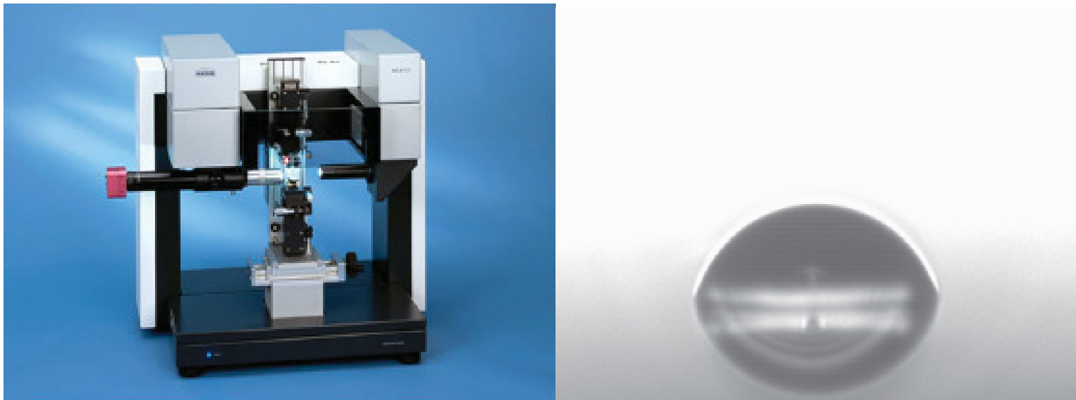

Figure 17: CA Measurement (left: measurement apparatus, right: liquid droplet with ca. 80 µm diameter).

For the calculation of the free surface energy the method after Owens-Wendt-Rabel-Kalble [24] has been used. According to the method, the surface tension was the sum of the dispersive and polar fractions: IFT = dispersive interfacial tension (IFT_D) + polar interfacial tension (IFT_P). CA measurements have been performed by Nurdogan Gürkan in the SPM Group Leoben.

3 Results

3.1 Investigation of substrate surfaces

3.1.1 Surface pre-treatment by plasma etching

The substrates used are single-side-polished p-type-doped (B) silicon wafers with native silicon oxide (resistivity 9-18 Ωcm), which provided by Infineon Technologies Austria AG. Three kinds of substrate samples after different surface pre-treatments were investigated: one was a sample without plasma etching and the others were pretreated by plasma etching for 50 seconds or 150 seconds.

For the rms roughness analysis, 5 µm×5 µm sizes were recorded in tapping mode at at least three independent locations for each sample. The σ values are the average of all these measurements and a standard deviation has been calculated from the individual data.

From fitting the Height-Height-Correlation function $C(x) = \sigma^2 \exp[-(|x|/\xi)^{2\alpha}]$ by using the software Origin, the lateral correlation length ξ and the roughness exponent α have been obtained as demonstrated in Figure 18.

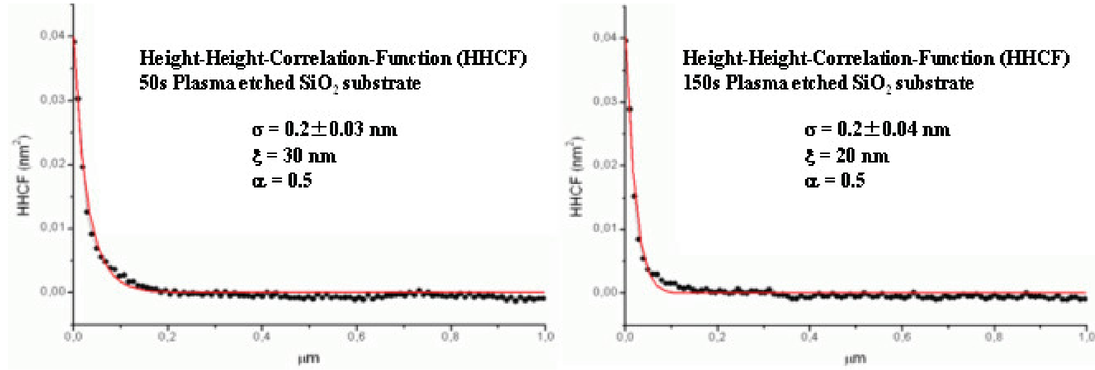

Figure 18: Calculations of σ, ξ, α by fitting the Height-Height-Correlation function $C(x) = \sigma^2 \exp[-(|x|/\xi)^{2\alpha}]$ demonstrated for 50s (left) and 150s (right) plasma etching, respectively.

In Figure 19, three 5 µm×5 µm topographical AFM images (z-scale is 10 nm) of samples, whose substrate surface experienced different plasma etching time, are presented. These three kinds of substrate surfaces show almost the same surface roughness quality.

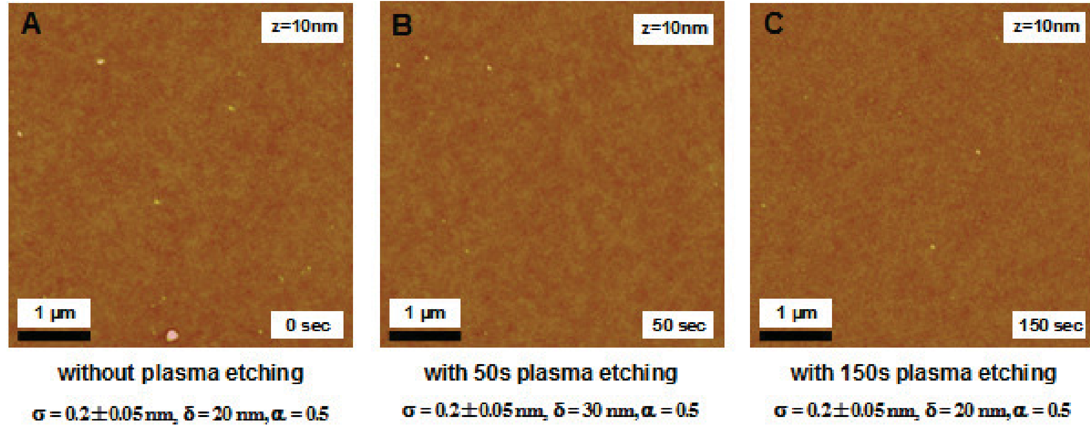

Figure 19: Surface roughness analysis of σ, δ, α after different plasma etching time (A: without plasma etching; B: after 50 seconds plasma etching; C: after 150 seconds plasma etching).

Figure 19A shows a smooth surface with some small contamination spots in a 5 µm×5 µm topography image. The surface roughness parameters $\sigma = 0.2 \pm 0.05$ nm, $\xi = 20$ nm, $\alpha = 0.5$ can be determined to demonstrate the surface quality of the surface without plasma etching. Figure 18B and Figure 18C show almost the same smooth surface morphology with some small contaminations on the substrate surface after 30 seconds or 150 seconds plasma etching. Their surface roughness parameters (50 seconds plasma etching: $\sigma = 0.2 \pm 0.05$ nm, $\xi = 30$ nm, $\alpha = 0.5$; 150 seconds plasma etching: $\sigma = 0.20 \pm 0.05$ nm, $\xi = 20$ nm, $\alpha = 0.5$) also show the same surface quality for different times of plasma etching.

3.3.2 Two different substrate types

As mentioned in chapter 2.1.1, two different kinds of substrate wafers were used for different characterization: a single-side-polished p-type-doped (B) silicon wafer with native silicon oxide (resistivity 9-18 Ωcm) here are called Infineon type, and a single-side-polished silicon wafer (n-type-doped (N/AS), resistivity < 0.003 Ωcm) with a thermally grown 165 nm thick silicon oxide layer produced by Sigert Consulting e.K, which are called Sigert type.
The photosensitive molecules Si-SCN were grown on these two different substrate surfaces. Using AFM measurement, surface topographical images are recorded to evaluate the film quality on both types of substrates.

3.3.2.1 Si-SCN surface layer unilluminated on the Infineon type substrate

Figure 20 shows the AFM results of the unilluminated SCN layer on the Infineon type substrate. For this homogeneous and smooth surface, some small contamination clusters are detected in both 5 µm×5 µm and 500 nm×500 nm topography images in Figure 20. The surface roughness parameters $\sigma = 0.3 \pm 0.05$ nm, $\xi = 15$ nm, $\alpha = 0.5$ demonstrated the Si-SCN surface quality on this Infineon type substrate.

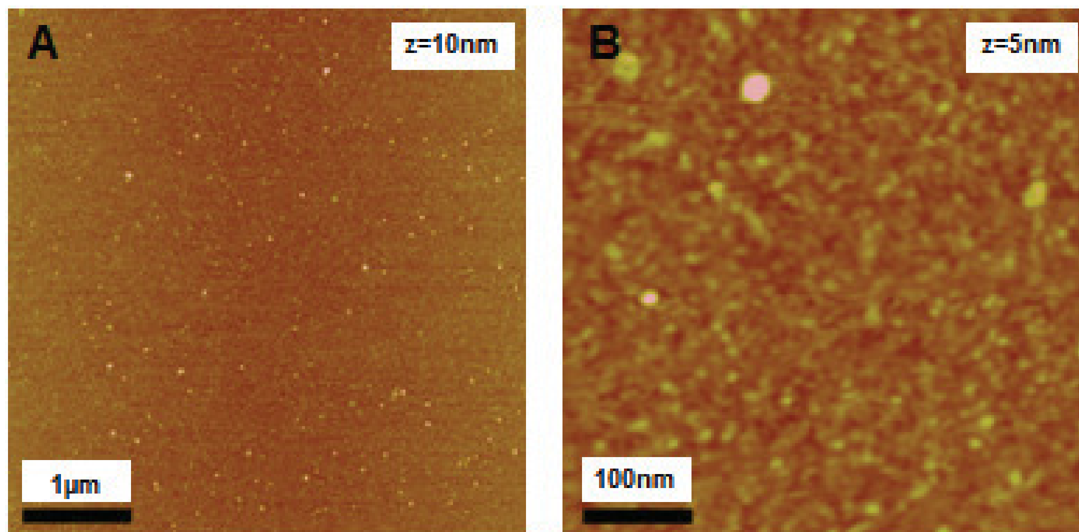

Figure 20: AFM topography images of the unilluminated SCN layer on the Infineon type substrate (A: 5 μm×5 μm image size; B: 500 nm×500 nm image size).

3.3.2.2 Si-SCN surface layer unilluminated on the Sigert type substrate

Figure 21 shows the AFM results of the unilluminated SCN layer on the Sigert type substrate. The same homogeneous and smooth surface with some small contamination clusters is detected in both 5 μm×5 μm and 500 nm×500 nm topography images. The surface roughness parameters σ = 0.4$\pm$0.05 nm, ξ = 30 nm, α = 0.5 can be determined to show the almost identical Si-SCN surface quality on this Sigert type substrate.

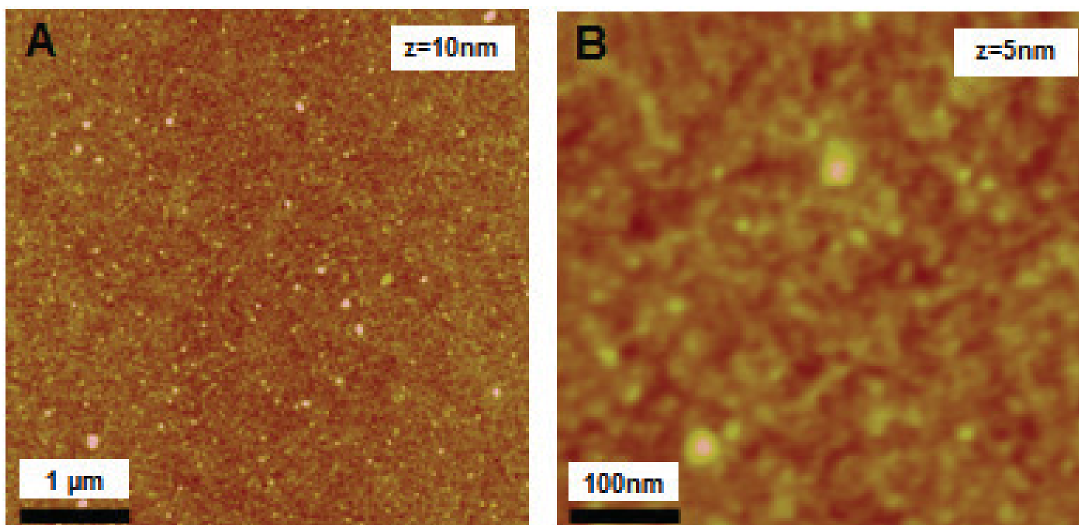

Figure 21: AFM topography images of the unilluminated Si-SCN layer on the Sigert type substrate (A: 5 μm×5 μm image size; B: 500 nm×500 nm image size).

3.2 Organic surface layers (PFDTS, CSTS)

3.2.1 Surface morphology without wiping process

In the chemical preparation processes of PFDTS and CSTS organic surface layers, the wiping step, which proceeds by a tissue drenched in toluene to wipe off the excessive surface molecules, was found to obtain a smother surface. First, we investigated some samples fabricated without wiping process. Using AFM measurements, a distinctive morphology of these surface layers can be detected.

3.2.1.1 PFDTS surface layer

Figure 22 shows AFM data for PFDTS surface layer which was formed by preparation Method 2 (in chapter 2.2.1.2) without wiping step. In AFM topography images, a "leopard-dapple" surface morphology, which is composed of many surface agglomerates and clusters, can be observed. This surface is rather inhomogeneous due to this leopard terrace formation. Therefore, the surface without wiping process is very rough with an rms roughness of $\sigma = 1.2 \pm 0.05$ nm.

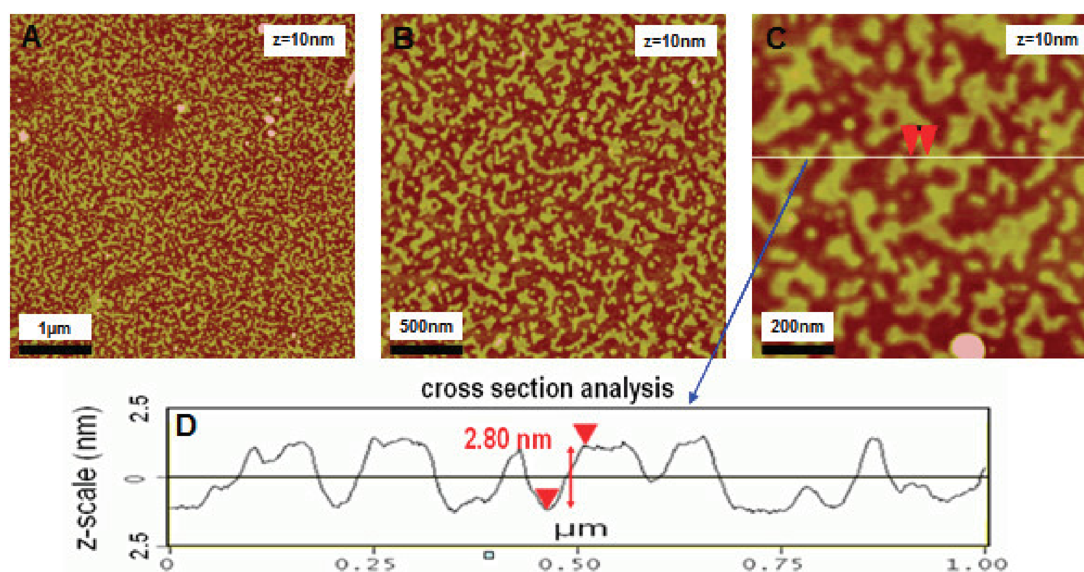

Figure 22: AFM topography images of PFDTS layers without wiping process (A: 5 μm×5 μm image size; B: 2.5 μm×2.5 μm image size; C: cross section on the 1 μm×1 μm topography image).

The height of this kind of leopard layer measured by cross section of the AFM image is about 2.8 nm (see Figure 22D), which is much higher than its intrinsic molecule length (PFDTS molecule length = 1.4 nm) and corresponds to an approximately 2 monolayer equivalent.

Comparing with the phase image in Figure 23, in the topography image the gold "leopard-dapple" terrace is the PFDTS layer and the brown part is the silicon oxide

substrate. From the cross section of both the AFM topography and phase images in blue line, where there is an obvious terraced morphology in Figure 23, the leopard terrace height for each monolayer is about 2 nm, which is little higher than its intrinsic molecule length of 1.4 nm.

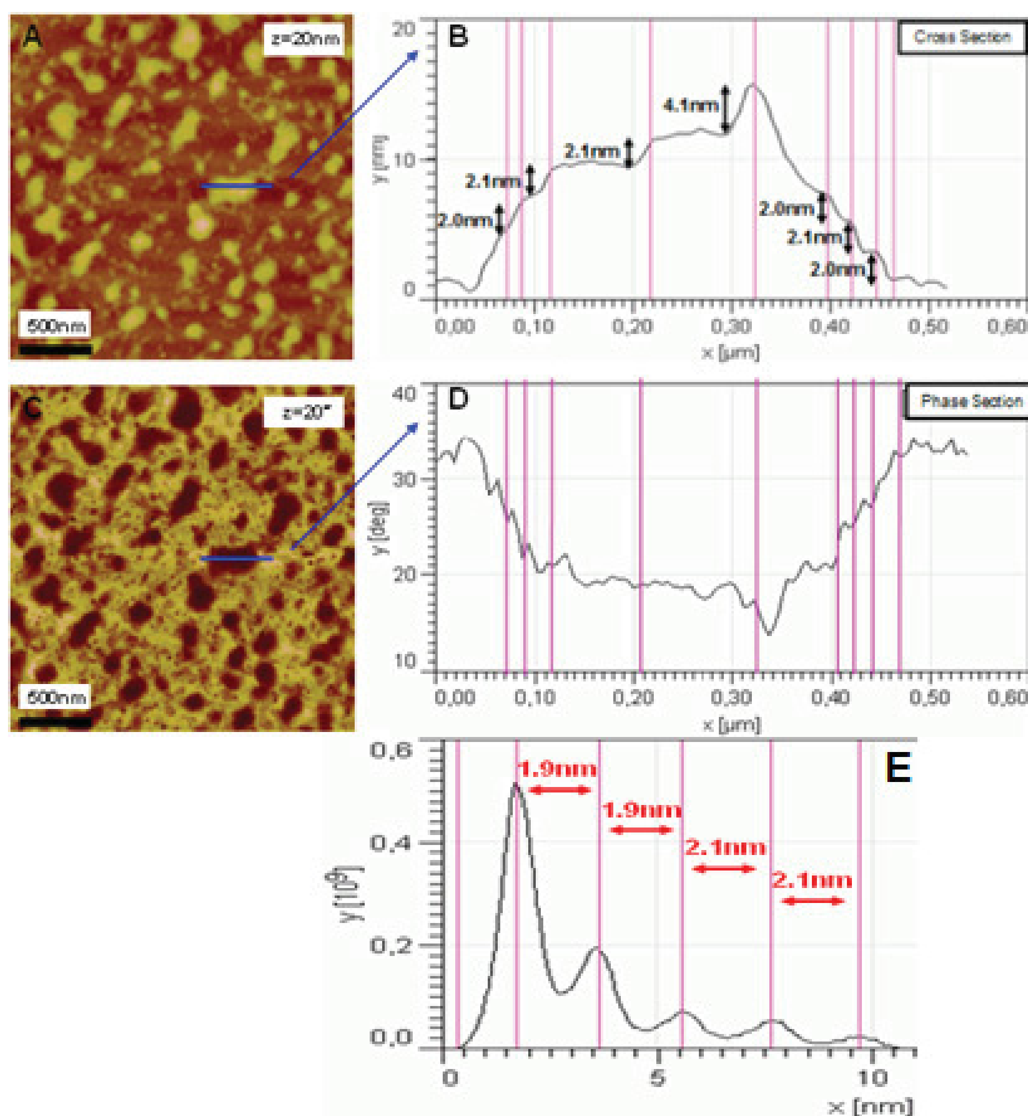

Figure 23: Cross sections in both AFM topography (A) and phase images (C) (A: 2.5 µm×2.5 µm topography image, z-scale = 20 nm; C: 2.5 µm×2.5 µm phase image, z-scale = 20°; B: cross section in A; D: phase section in C; E: height distribution of the topography image A of PFDTS layer).

The height distribution was determined from Figure 23A and is presented in Figure 23E. Through the height distribution calculation of the topography image data by AFM software, the average height of each PFDTS terrace is almost the same about 2 nm (see Figure 23E), which is corresponding to the molecule length. This kind of multilayer leopard terrace surface morphology can be explained by other stable and ordered structures, which perhaps consist of a tail-to-tail group combination.

3.2.1.2 CSTS surface layer

This CSTS surface layer was formed without wiping step. In the AFM topography images provided in Figure 24, we can find a lot of round surface agglomerates and clusters (diameter: up to 300 nm; height: up to 70 nm) on the surface. Similar to the PFDTS surface without wiping, this CSTS surface without wiping process is also very rough and its rms roughness is $\sigma = 3.6 \pm 0.8$ nm.

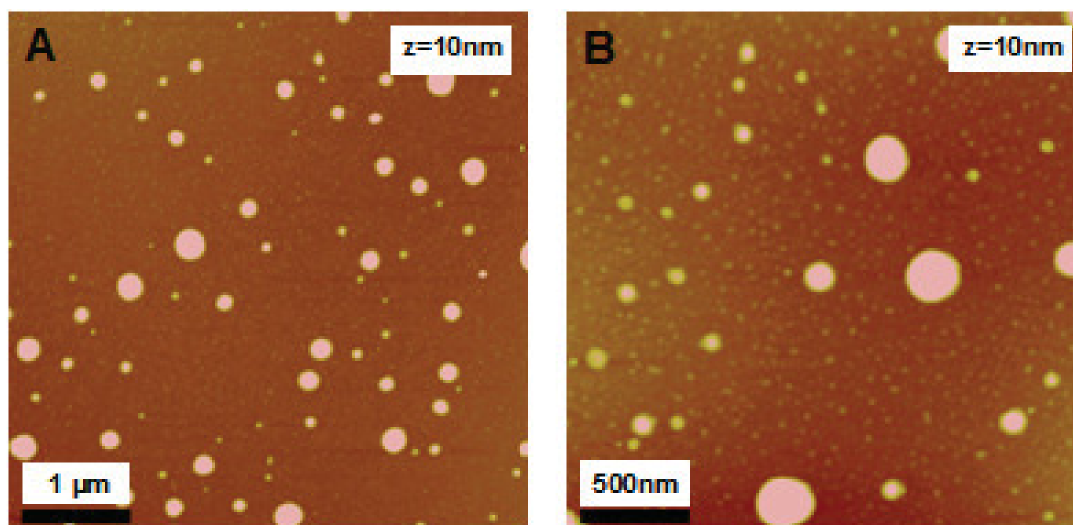

Figure 24: AFM topography images of CSTS layers without wiping process (A: 5 µm×5 µm image size, B: 2.5 µm×2.5 µm image size; z-scale = 10 nm).

The thickness of CSTS surface layer can be obtained in the XRR measurements. The film thickness is different when the film grows under dry inert gas condition or under ambient condition: The layer made under dry condition has a thickness of 2.4 nm, which corresponds to about 2.5 monolayer equivalents. The layer grown under ambient conditions has a thickness of 11 nm, which corresponds to about 11.5 monolayer equivalents. In ambient air, the residual humidity can lead to an increase of thickness. Further, the increased water content can result in a fast hydrolysis of the $SiCl_3$ groups and thus the formation and subsequent deposition of oligomeric siloxane clusters or multilayers [4].

3.2.2 Comparison of 3 different methods after the wiping process

In chapter 2.2 the three different sample preparation methods of PFDTS and CSTS surface layer have been described. As mentioned above, prior to the wiping process the formed surface layer is very rough. The leopard terrace surface morphology in the PFDTS surface and the round cluster surface morphology in the CSTS surface can be obviously detected. It is assumed that the wiping process by using a tissue drenched in toluene will result in a smoother organic surface layer.

3.2.2.1 PFDTS surface layer

1) The surface morphology of the PFDTS surface layer, which was formed by Method 1 after a wiping step, is shown in Figure 25. In these AFM topography images a broad band, which was obviously formed by the wiping process, can be observed. In this wiped band the excessive surface molecules were wiped off by a tissue and the rms roughness σ in this area is $\sigma = 0.3$ nm which is significantly lower than one of the no-wiped areas ($\sigma = 0.5 \pm 0.05$ nm).

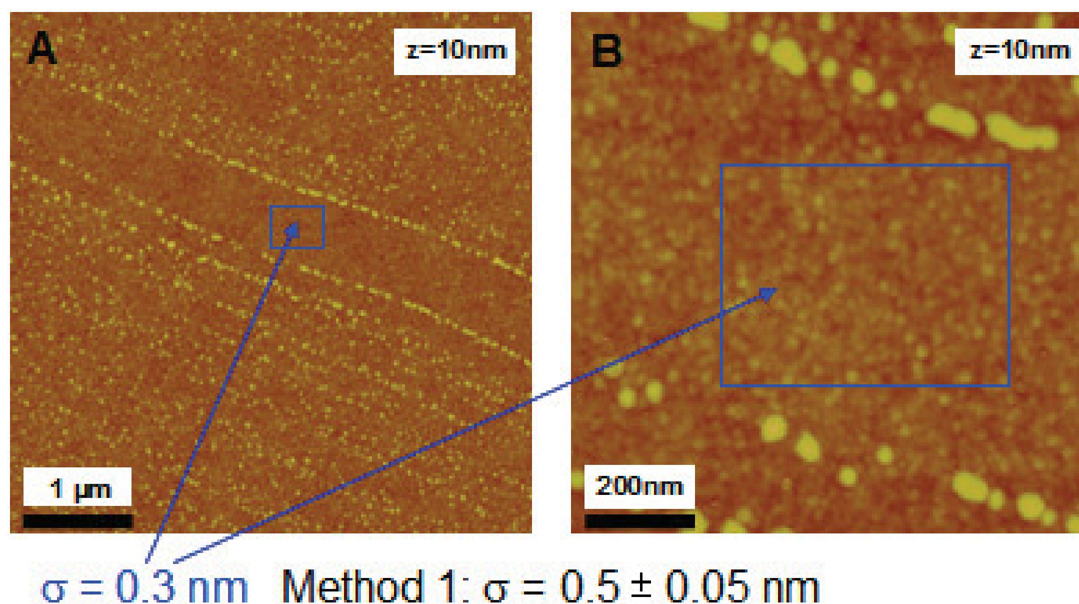

Figure 25: The AFM topography images of the wiped PFDTS surface after Method 1 (A: 5 µm×5 µm image size, B: 1 µm×1 µm image size; z-scale = 10 nm, blue rectangles mark the area in the wiped band).

2) The surface morphology of the PFDTS surface layer, which was formed by Method 2 after a wiping step, is shown in Figure 26. In both AFM topography images, there are no broad wiping bands but some small clusters (diameter: ca. 25 nm) visible on the surface. The rms roughness σ is 0.3 ± 0.05 nm. Thus, the surface after Method 2 is smoother than the one after Method 1.

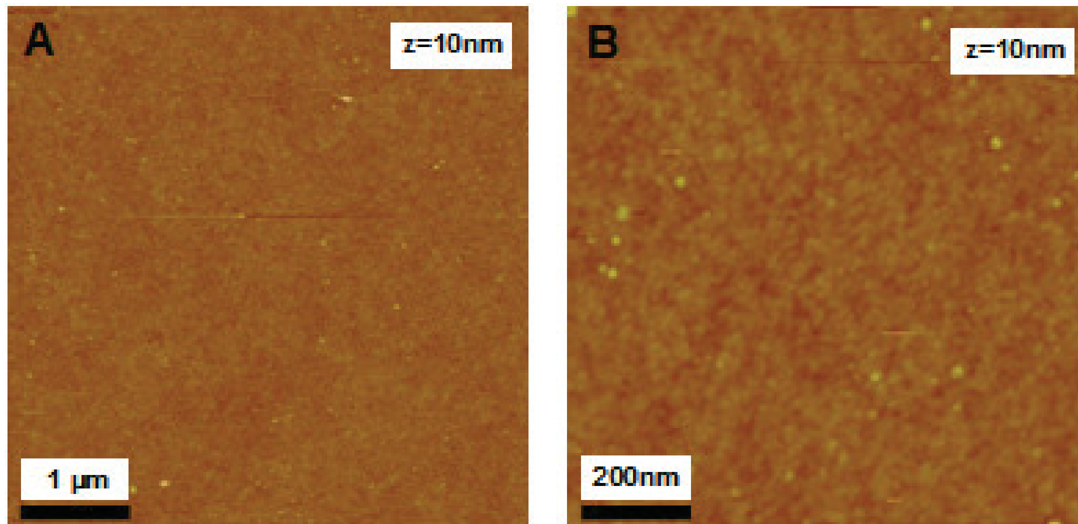

Figure 26: The AFM topography images of the wiped PFDTS surface after Method 2 (A: 5 µm×5 µm image size, B: 1 µm×1 µm image size; z-scale = 10 nm).

3) The surface morphology of the PFDTS surface layer, which was formed by Method 3 after a wiping step, is shown in Figure 27. The surface after Method 3 is similar to the one after Method 1. In the presented AFM topography images a wiped band can be detected. In this wiped band, the excessive surface molecules were wiped off by a tissue, and the rms roughness σ within the band (σ = 0.3 nm) thus is lower than one of the non-wiped areas (σ = 0.4 ± 0.05 nm).

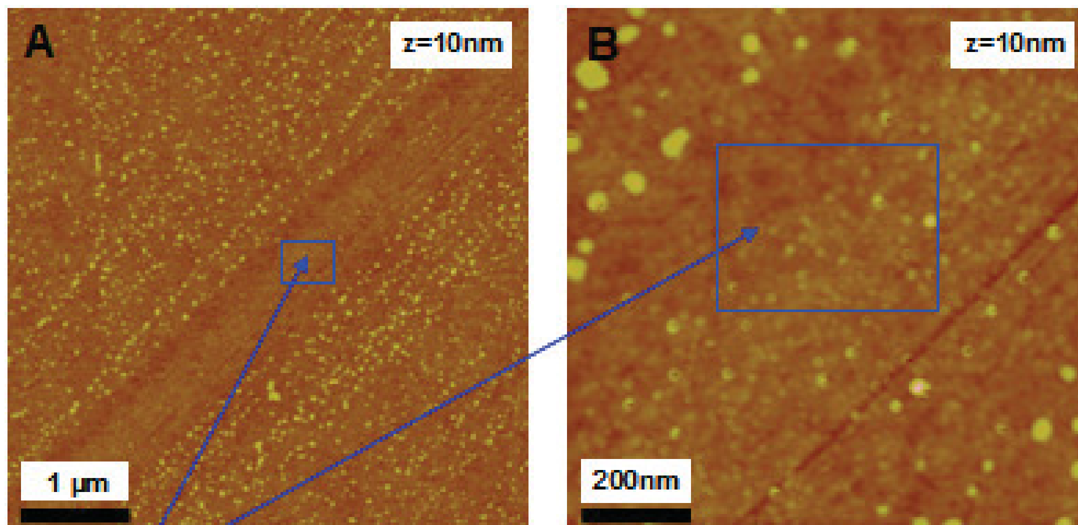

Figure 27: The AFM topography images of the PFDTS surface after Method 3 (A: 5 µm×5 µm image size, B: 1 µm×1 µm image size; z-scale = 10 nm, blue rectangles indicate the area in the wiped band).

3.2.2.2 CSTS surface layer

1) The surface morphology of the CSTS surface layer, which was formed by Method 1 after a wiping step, is shown in Figure 28. The AFM topography images reveal that the surface after Method 1 is smooth and its rms roughness σ is 0.3±0.1nm. There are also very small clusters (diameter: ca. 20 nm) on the surface.

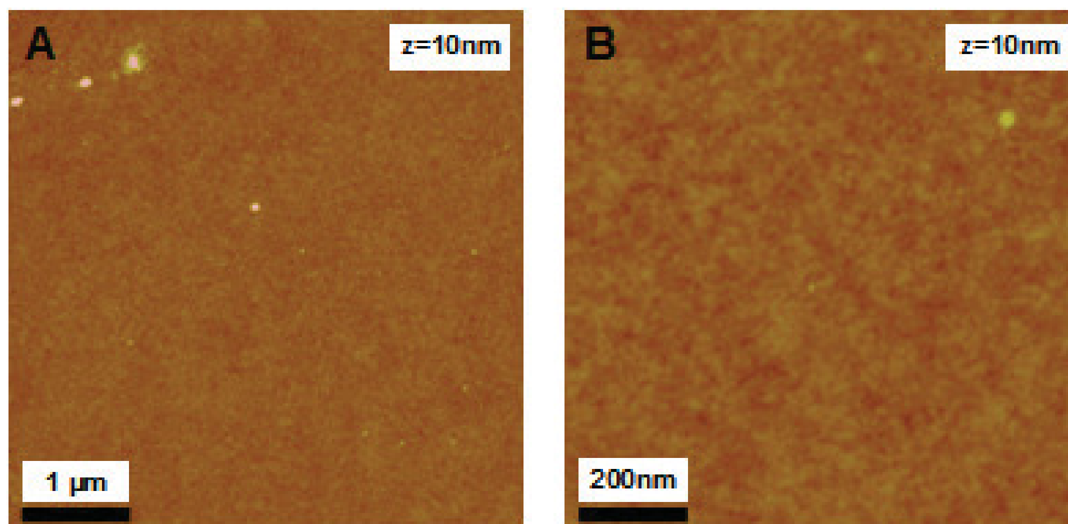

Figure 28: The AFM topography images of the CSTS surface after Method 1 (A: 5 µm×5 µm image size, B: 1 µm×1 µm image size; z-scale = 10 nm).

2) The surface morphology of the CSTS surface layer, which was formed by Method 2 after a wiping step, is shown in Figure 29. The surface after Method 2 is also very smooth with an rms roughness σ is 0.3±0.1 nm. There are also some very small clusters on the surface with a diameter of ca. 25 nm.

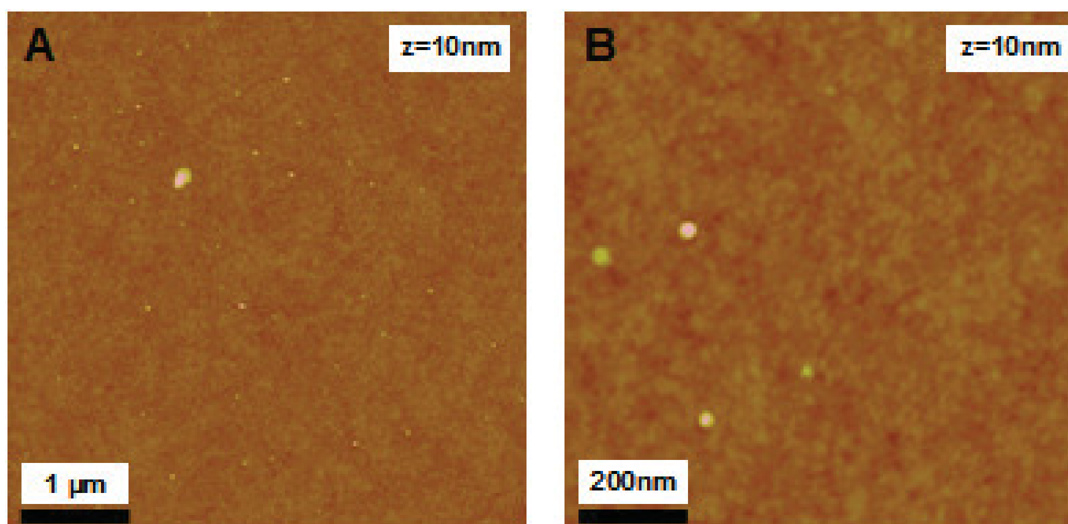

Figure 29: The AFM topography images of the wiped CSTS surface after Method 2 (A: 5 µm×5 µm image size, B: 1 µm×1 µm image size; z-scale = 10 nm).

3) The surface morphology of the CSTS surface layer, which was formed by Method 3 after a wiping step, is presented in Figure 30. The surface after Method 3 is rougher than the one after Method 1 and 2. In the AFM topography images, the wiped bands are not clearly observed. The difference of the rms roughness in the wiped and non-wiped areas is not obvious and the rms roughness σ of this surface is 0.5 ± 0.05 nm.

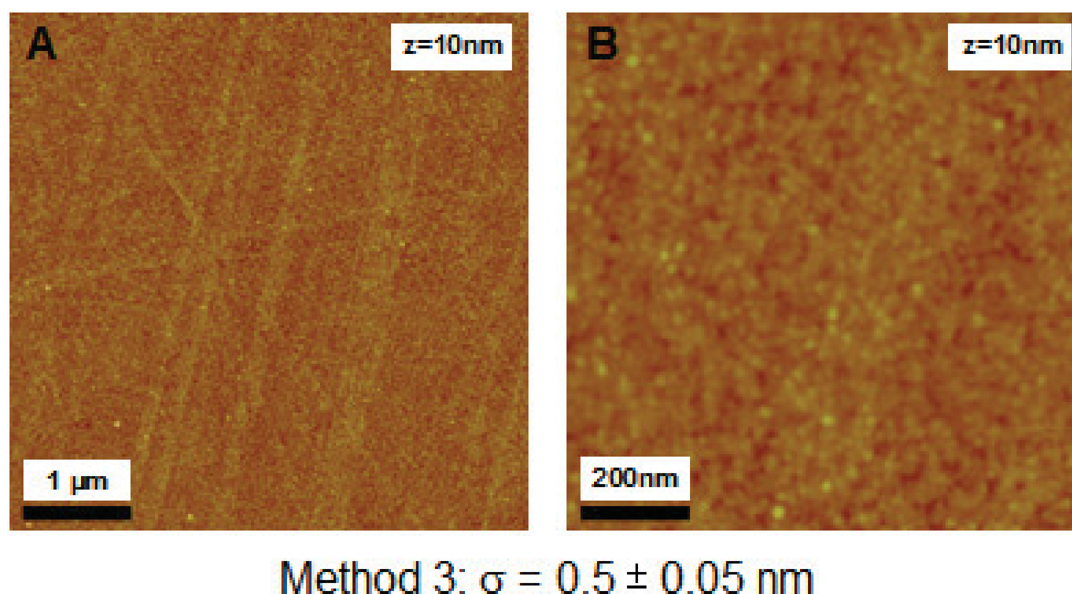

Figure 30: The AFM topography images of the wiped CSTS surface after Method 3 (A: 5 µm×5 µm image size, B: 1 µm×1 µm image size; z-scale = 10 nm).

3.2.2.3 CA measurements of PFDTS and CSTS surface layers:

Using CA measurements with water drops, the corresponding CA results of different sample (SiO_2 substrate, PFDTS and CSTS) surfaces after three different preparation methods are recorded as follows:

1) CA of SiO_2 substrate surface: Method 1: 40°; Method 2: 40°; Method 3: 40°.
2) CA of PFDTS surface: Method 1: 99°; Method 2: 100°; Method 3: 101°.
3) CA of CSTS surface: Method 1: 33°; Method 2: 35°; Method 3: 79°.

3.3 Photoreactive thin layers

3.3.1 Surface morphology for different deposition, concentration, and time

During the chemical preparation processes, after the pre-treatments of plasma etching and a deionized water dip, the clean substrate wafers were immersed into a different Si-SCN solution concentration (0.01 vol% or 0.1 vol%) in HPLC-grade toluene at

room temperature under ambient conditions for different time intervals (16 hours or 1 week). Through the comparison with different samples by using AFM measurements, the correlation between surface morphology and the layer fabrication conditions can be determined.

3.3.1.1 The lying sample

After the pre-treatment process, the substrate wafers were immersed into a Si-SCN solution. These substrates were lying in the solution during the sample deposition process. Using AFM, the surface morphology after different deposition conditions has been recorded. The corresponding surface roughness parameters (rms roughness σ, lateral correlation length ξ and the roughness exponent α) are determined as follows:

1) The substrate wafers were immersed into a 0.01 vol% Si-SCN solution for 1 week. In both 5 µm×5 µm and 500 nm×500 nm topography images in Figure 31, some small contamination clusters are found on this surface. The surface roughness parameters $\sigma = 0.7 \pm 0.1$ nm, $\xi = 15$ nm, $\alpha = 0.5$ can be obtained to show this surface quality. The preferential feature size (diameter: 10 nm; height: 3 nm) on the surface can be detected.

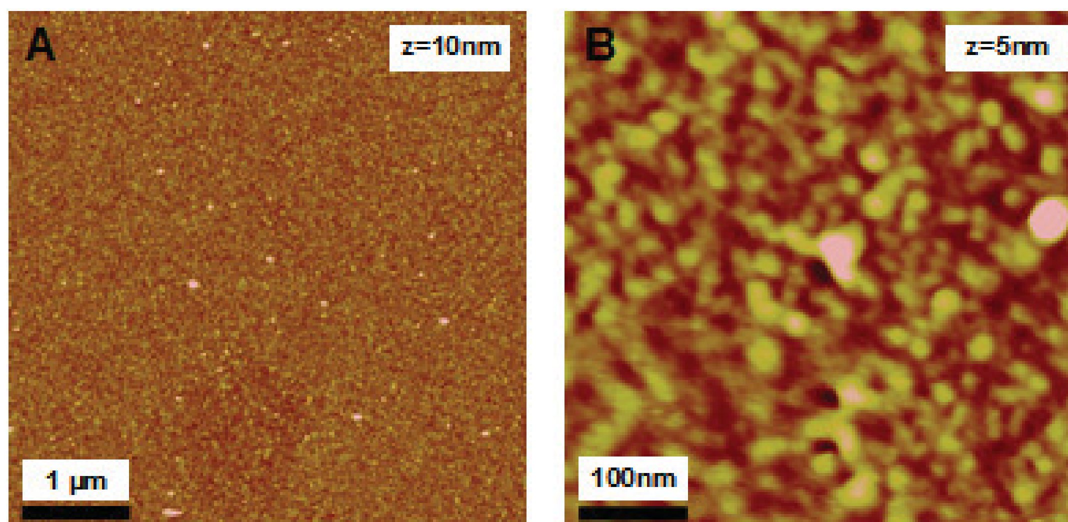

Figure 31: Sample lying preparation in 0.01 vol% SCN-solution for 1 week deposition (AFM topography images: A: 5 µm×5 µm image size; B: 500 nm×500 nm image size).

2) The substrate wafers were immersed into a 0.1 vol% Si-SCN solution for 16 hours. In both 5 µm×5 µm and 500 nm×500 nm topography images in Figure 32, some small contamination clusters are also found on this surface. The surface roughness parameters σ = 1.5±0.05 nm, ξ = 20 nm, α = 0.5 can be obtained to show the less surface quality than surface in Figure 31.

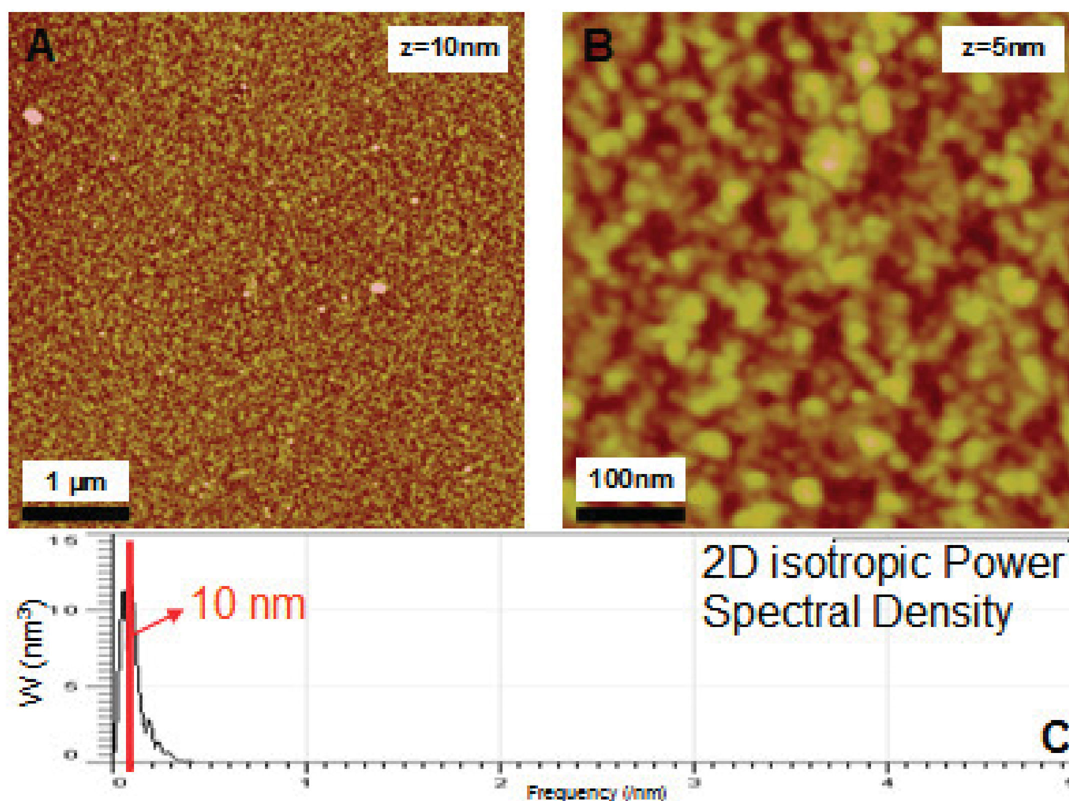

Figure 32: Sample lying preparation in 0.1 vol% SCN-solution for 16 hours deposition (AFM topography images: A: 5 µm×5 µm image size; B: 500 nm×500 nm image size; C: 2D isotropic power spectral density on the B surface).

The Power Spectral Density plot in Figure 32C shows a peak which corresponds in real space to 10 nm lateral feature size. Their average height has been determined to be about 2 nm.

3.3.1.2 The standing sample

In this sample preparation process, the substrate wafers were standing in a 0.1vol % Si-SCN solution for 16 hours. Figure 33 shows the 5 µm×5 µm and 500 nm×500 nm AFM topography images. A few small contamination clusters (diameter: ca. 30 nm; height: 6 nm) are found on the surface. The surface roughness parameters σ = 0.4± 0.05 nm, ξ = 30 nm, α = 0.5 can be obtained.

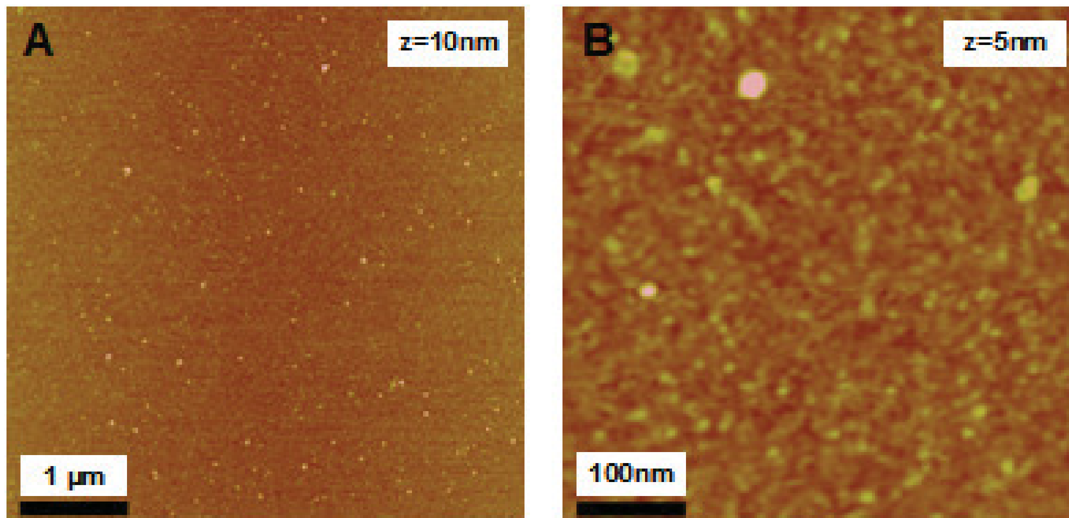

Figure 33: Sample standing preparation in 0.1 vol% SCN-solution for 16 hours deposition (AFM topography images: A: 5 µm×5 µm image size; B: 500 nm×500 nm image size).

3.3.2 Surface morphology after post modification

After UV illumination of the Si-SCN surface, the post modification reactions with PA or NH_3 proceeded on the isomerized Si-NCS surface termination that can be modified to different surface terminations, which are called PA and amine (NH_3) terminations. Using the AFM and CA measurements, the surface characterization changes due to the post modification can be observed. The surface information, which consists of roughness parameters (rms roughness σ, lateral correlation length ξ and the roughness exponent α), CA and surface energy, are obtained as follows:

1) Si-SCN surface layer after post modification with NH_3

This smooth surface with some small contamination clusters are detected in both 5 µm×5 µm and 500 nm×500 nm topography images in Figure 34. The surface of the modified Si-SCN surface layer shows a uniform and rather featureless topography. The surface roughness parameters σ = 0.3$\pm$0.05 nm, ξ = 35 nm, α = 0.5, CA (using water droplets) and surface energy results can be determined to confirm the qualitative observation of the surface layer: α_{water} = 73°; $\alpha_{water\ /\ toluene}$ = 89° (after cleaning with toluene); IFT_D = 30.9; IFT_P = 0.7.

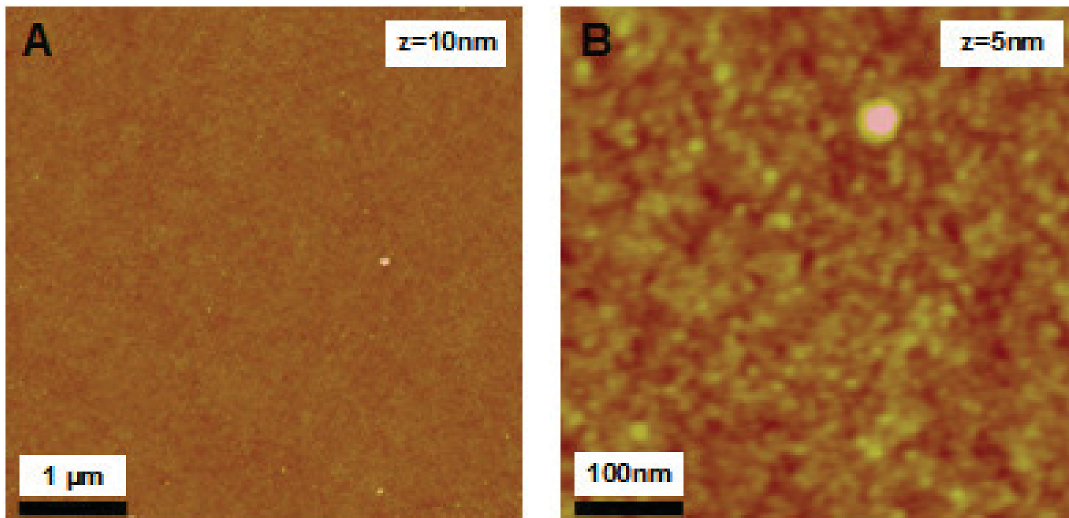

Figure 34: AFM topography images of Si-SCN surface layer illuminated after modification with NH_3 (A: 5 µm×5 µm image size; B: 500 nm×500 nm image size).

2) Si-SCN surface layer illuminated after post modification with PA

Figure 35 shows that the smooth surface with some small contamination clusters (diameter: up to 50 nm; height: 3.5 nm) is detected in both 5 µm×5 µm and 500 nm×500 nm AFM topography images. Besides the contaminations, the surface of the modified Si-SCN surface layer shows a uniform featureless topography. The surface roughness parameters $\sigma = 0.3 \pm 0.05$ nm, $\xi = 25$ nm, $\alpha = 0.5$, CA (using water droplets) and surface energy results can be determined to confirm the qualitative observation of the surface layer: $\alpha_{water} = 73°$; $\alpha_{water\,/\,toluene} = 90°$ (after cleaning with toluene); $IFT_D = 29.2$; $IFT_P = 1.3$.

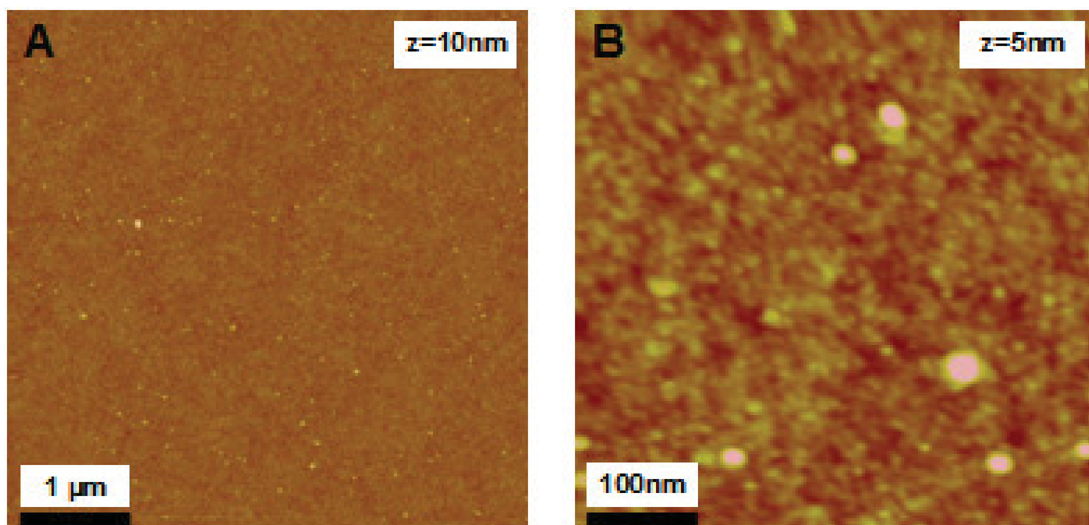

Figure 35: AFM topography images of Si-SCN surface layer illuminated after modification with PA (A: 5 µm×5 µm image size; B: 500 nm×500 nm image size).

3.3.3 Friction force contrast patterns after UV illumination through different stripe masks

In this part of the thesis, the photoreaction was carried out in combination with lithographic techniques to demonstrate the preparation of micro-patterned functionalized layers [6]. For this purpose, contact masks with different equidistant lines and spaces (3 µm, 5 µm and 10 µm) were placed on the Si-SCN surface layer and illuminated with UV light (254 nm, 80 $mJcm^{-2}$) under inert gas. During the photo-induced isomerization process, only the uncovered surface with photoreactive SCN group can be changed to the corresponding NCS groups during the illumination with UV light. By this approach, a patterned structure, which is composed of alternating stripes of Si-SCN and Si-NCS surface terminations, was formed on this surface layer.

In order to reveal a material's contrast between illuminated and non-illuminated regions of the patterned surface, FFM measurements were performed under ambient conditions. In this case we can display friction pattern contrast in different length scale by FFM measurements. In the following, we present the FFM images of illuminated Si-SCN surface layers using three different contact masks with different equidistant lines, which are depicted in Figures 36 and 37. In chapter 2.2.2.1.4, we have mentioned that the kinetic investigations of liquid films of Si-SCN by FTIR spectroscopy show that only 25-30% NCS surface termination is formed because the side reactions after the UV illumination process. Therefore, in the topographical image, no structural features due to the patterning process are clearly discernible because a height difference of approximately 1 nm (approximately 20% of the initial layer thickness) [25] within a lateral distance of 10 µm or 20 µm periodicity of the stripe pattern can hardly be analyzed [6]. However, an evident stripe pattern of areas with low and high friction appears in the friction images. These parallel stripes have a period, which is in agreement with the dimension of the contact mask used for the patterning process. In all friction images presented, bright areas correspond to higher friction and dark areas mean lower friction. The isomerization leads to a chemical change of the surface termination (Si-SCN to Si-NCS). Moreover, the yield of the Si-NCS is only 25-30% after UV illumination. Thus, in the friction images the borderlines of the stripes are not straight and clear because of the slight material contrast between the Si-SCN and Si-NCS stripes. The further chemical identification of the stripes will be discussed in section 4.7.

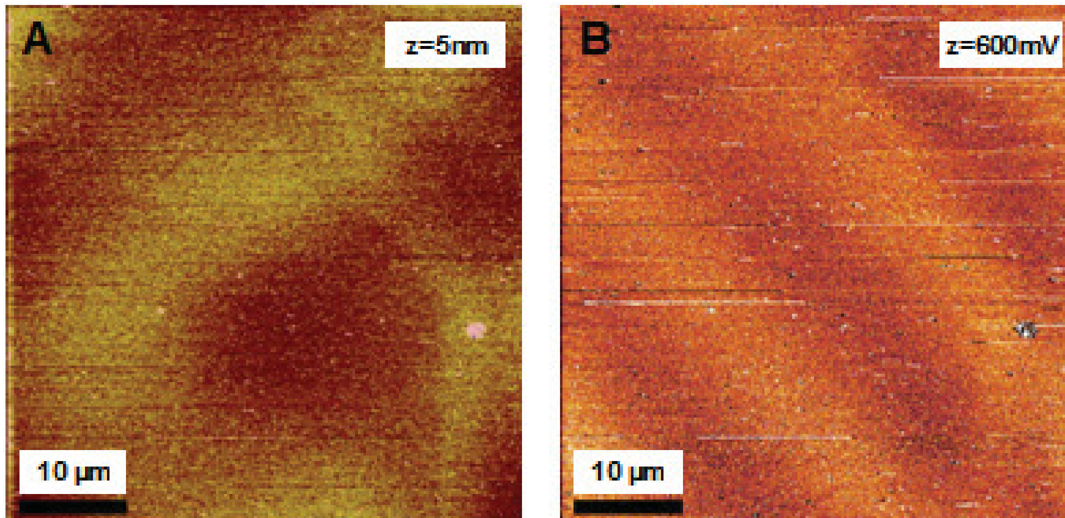

Figure 36: AFM results of Si-SCN surface layer after illumination through a 10 µm stripe mask (A: 50 µm×50 µm topography image with 5 nm z-scale; B: alternating 10 µm broad stripes pattern of SCN and NCS in the FFM image).

Figure 36 shows for the 10 µm mask the topography image (A) and the friction image (B) recorded by FFM. In the 50 µm×50 µm topography image (z-scale = 5 nm), no structural features resulting from the patterning process are visible. The real morphology undulation and some contaminations can be observed in topography image. However, in the 50 µm×50 µm friction image (z-scale = 600 mV, set point = 0.2 V), a clear stripe pattern consisting of alternating 10 µm high friction stripes and 10 µm low friction stripes, which is corresponding to the dimension of the 10 µm contact mask used for the patterning process, is discernible. Because of the slight friction force contrast between the Si-SCN and Si-NCS stripes, the borderlines of the pattern stripes are not straight and clear.

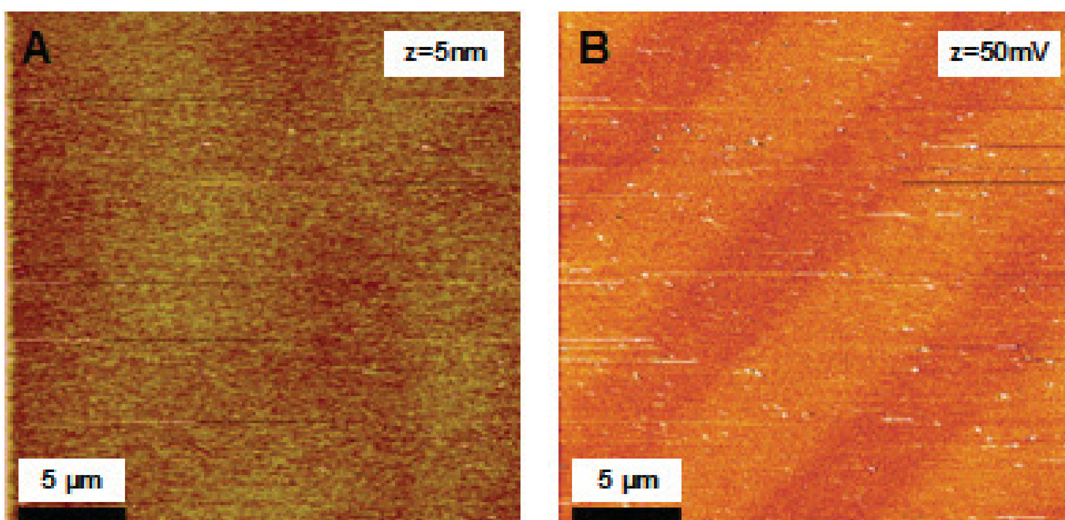

Figure 37: AFM results of Si-SCN surface layer after illumination through a 5 µm stripe mask (A: 15 µm×15 µm topography image with 5 nm z-scale; B: alternating 5 µm broad stripes pattern of SCN and NCS in the FFM image).

Figure 37 shows for the 5 µm mask the topography image (A) and the friction image (B) recorded by FFM. In 15 µm×15 µm topographical image (z-scale = 5 nm), no structural features resulting from the patterning process are visible. The real morphology undulation and some contamination spots can be also seen in the topography image. However, in the 15 µm×15 µm friction image (z-scale = 50 mV, set point = 0.5 V), a clear stripe pattern consisting of alternating 5 µm high friction stripes and 5 µm low friction stripes can be found. The bright stripes mean higher friction and dark stripes correspond to low friction.

3.3.4 Friction force contrast patterns after post modification through different stripe masks

At Graz University of Technology, the photoisomerization as well as the post modification reactions with gaseous amines were monitored by XPS measurement. The XPS measurement shows that the post modification with PA results only in a slight change in the XPS spectra because of the low yield of the NCS in photoisomerization process (approximately 30%). Because fluorine can be detected easily by XPS [6], FA was also chosen as a reactant for post modification to obtain a better signal of the post modification in XPS measurement.

3.3.4.1 Modification with PA after UV illumination

After the photoisomerization process, the contact mask was removed from the Si-SCN/Si-NCS patterned surface, and then the surface layer was exposed to vapor of PA. During the post modification with PA, on the surface layer only the NCS surface termination can react with the PA to form the corresponding PA surface termination. This new termination has a different level of friction in comparison to the SCN surface termination. Using the FFM measurement, the surface information on topography and friction on this patterned surface is obtained. Figure 38 shows the results of corresponding FFM measurements.

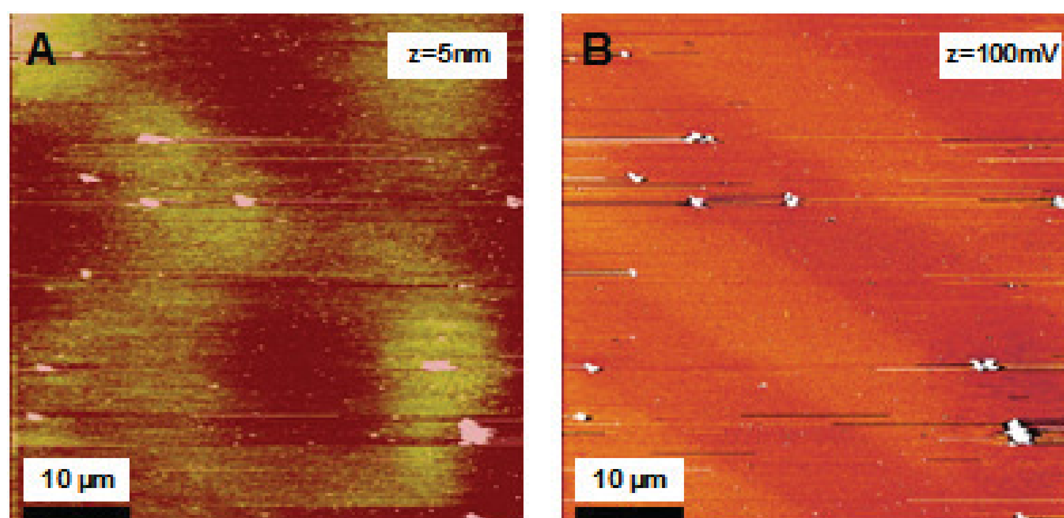

Figure 38: AFM results of Si-SCN surface layer after illumination and modification with PA through a 10 µm stripe mask (A: 50 µm×50 µm topography image with 5 nm z-scale; B: alternating 10 µm broad stripes pattern of SCN and PA in FFM image).

Figure 38 shows the topography image (A) and the friction image (B) recorded by FFM. There is a weak stripe pattern visible with the expected 10 μm spacing in the 50 μm×50 μm topography image (z-scale = 5 nm). This structural feature is rather weakly visible because of the evident real morphology undulations and several surface contaminations, which interfere with the tip scanning on the surface. However, clear 10 μm wide alternating stripes of two different friction levels can be detected in the 50 μm×50 μm friction image (z-scale = 100 mV, set point = 0.3 V). Clear stripe pattern in the friction image corresponds to the weakly visible stripe pattern in the topography image. Through the pattern features in the topography image and the corresponding relation with the friction image, the chemical identification of the stripe pattern is possible and will be described in chapter 4.7. Because friction force contrast between the Si-SCN and Si-PA stripes is higher than the contrast between Si-SCN and Si-NCS stripes after the post modification, the borderlines of the pattern stripes are straighter than the ones of the only illuminated patterned surface. Moreover, a surface contamination like in the lower right corner of the topography image can lead to a large disturbed area, in which there is no clear friction contrast available.

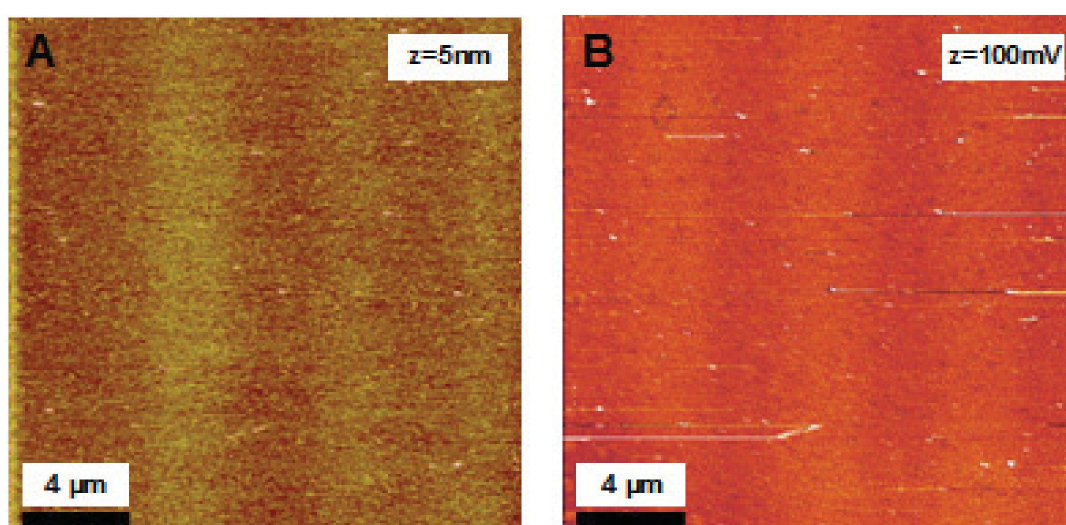

Figure 39: AFM results of Si-SCN surface layer after illumination and modification with PA through a 3 μm stripe mask (A: 20 μm×20 μm topography image with 5 nm z-scale; B: alternating 3 μm broad stripes pattern of SCN and PA in the FFM image).

Figure 39 shows that similar clear results are also obtained for the application of a 3 μm mask in the patterned process. In the 20 μm×20 μm topographical image (z-scale = 5 nm), there is a weak stripe pattern visible with the expected 3 μm spacing. Friction contrast stripes, which correspond to the topographic stripes, can be detected in friction image (z-scale = 100 mV, set point = 0.9 V). There are also many surface contaminations to interfere the friction mechanisms.

3.3.4.2 Modification with FA after UV illumination

During the post modification with FA, on the surface layer only the NCS surface

termination can react with the FA to form corresponding FA surface termination, which has a different level of friction in comparison in SCN surface termination. This is clearly demonstrated by the FFM investigation as presented in Figure 40.

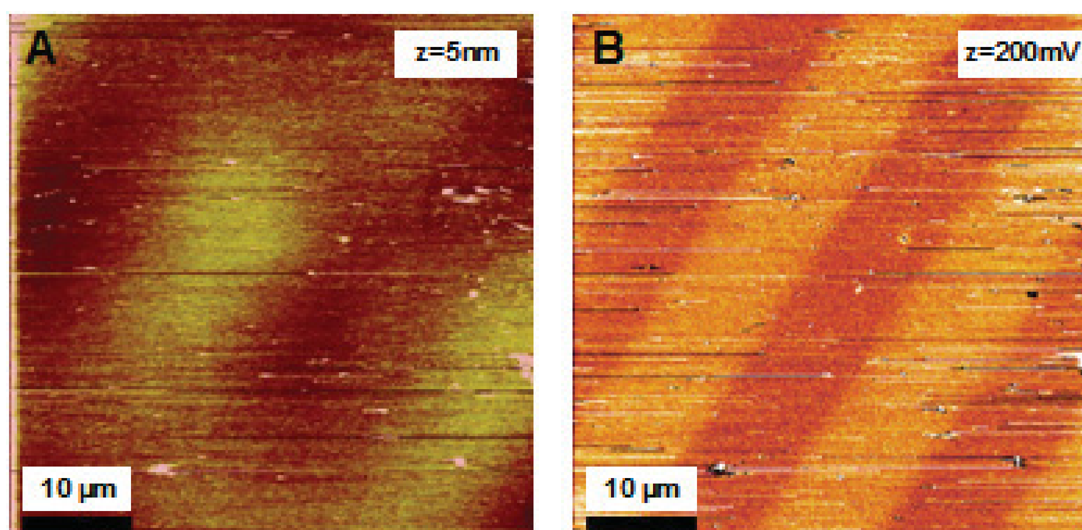

Figure 40: AFM results of Si-SCN surface layer after illumination and modification with FA through a 10 µm stripe mask (A: 50 µm×50 µm topography image with 5 nm z-scale; B: alternating 10 µm broad stripes pattern of SCN and FA in FFM image).

In the 50 µm×50 µm topographical image (see Figure 40A), there is no stripe pattern with the expected spacing visible because of the interference with large-area surface morphology corrugations. However, clear 10 µm wide alternating stripes of two different friction levels are detected in the 50 µm×50 µm friction image (z-scale = 200 mV, set point = 0.9 V). Because the friction force contrast between the Si-SCN and Si-FA stripes is higher than the contrast between Si-SCN and Si-NCS stripes after the post modification, the borderlines of the stripes are straighter than the ones of the only illuminated patterned surface. A lot of surface contaminations can lead to unclear disturbed scan lines in the friction image.

Figure 41 shows the corresponding AFM results for the 5 µm mask. In the friction image (z-scale = 50 mV, set point = 0.2 V), clear 10 µm wide alternating stripes of two different friction levels are detected. The interference with contaminations is also found. The friction contrast is lower than for the surface modified by using the 10 µm wide mask, but still clearly detectable.

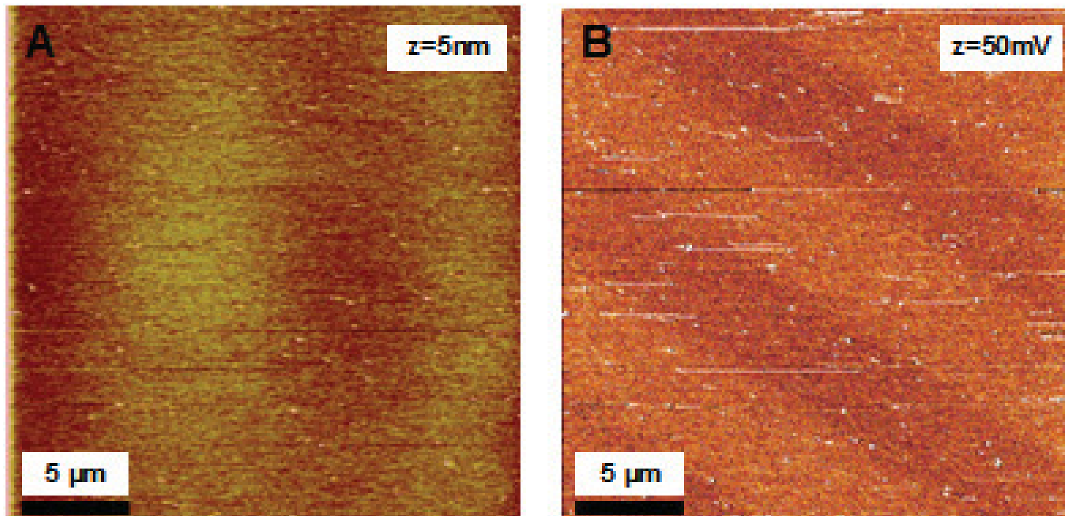

Figure 41: AFM results of Si-SCN surface layer after illumination and modification with FA through a 5 µm stripe mask (A: 25 µm×25 µm topography image with 5 nm z-scale; B: alternating 5 µm broad stripes pattern of SCN and FA in the FFM image).

Finally, Figure 42 shows the results for using the 3 µm mask. In the friction image (z-scale = 100 mV, set point = 0.9 V), a clear contrast related to the 3 µm mask pattern is still detectable.

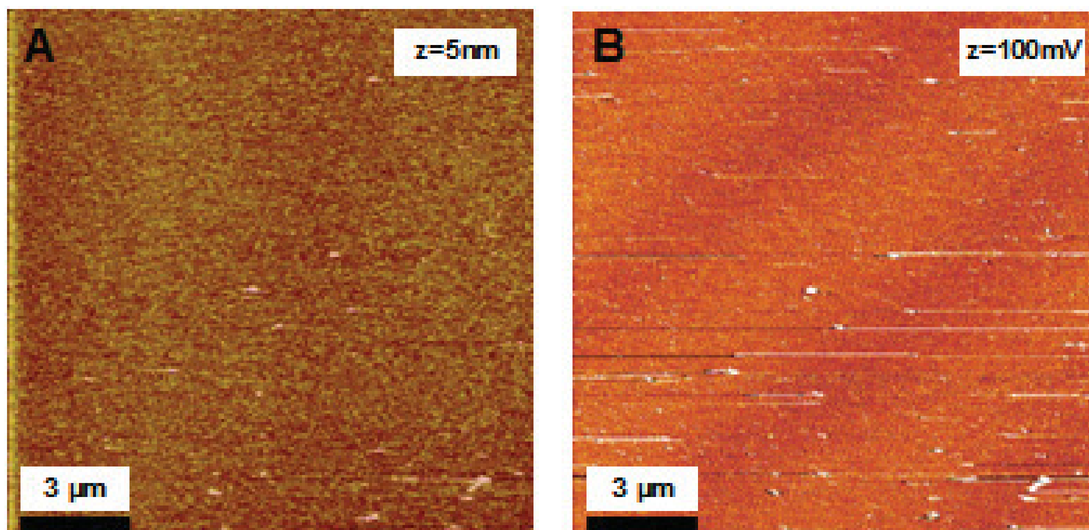

Figure 42: AFM results of f Si-SCN surface layer after illumination and modification with FA through a 3 µm stripe mask (A: 15 µm×15 µm topography image with 5 nm z-scale; B: alternating 3 µm broad stripes pattern of SCN and FA in the FFM image).

3.3.5 Friction force contrast after applying two crossed masks

In this final experiment, the patterned surface was formed by two UV illuminations using crossed masks with an intermediate post modification step with PA. The surface preparation process is sketched in Figure 43.

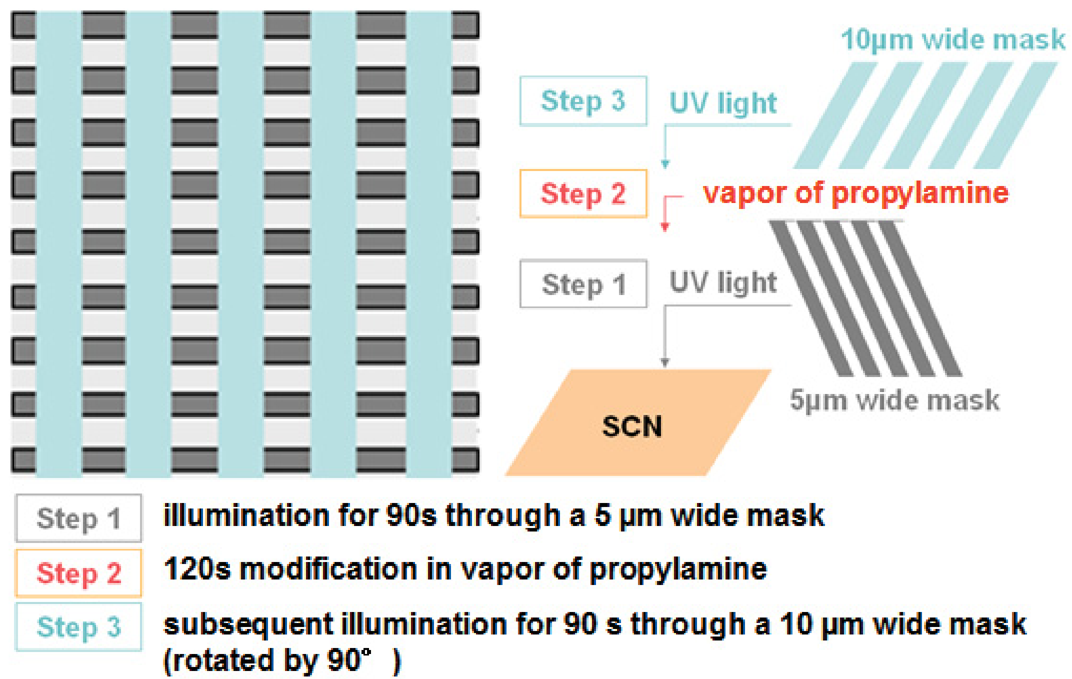

Figure 43: Scheme of the surface preparation process using crossed masks.

This preparation process consists of three steps: in the first step, the Si-SCN surface layer was illuminated with UV light using a mask with 5 µm lines and 5 µm spaces. Thus, a sequence of 5 µm pristine Si-SCN stripes and illuminated Si-NCS stripes are formed on the surface. In the second step, this patterned surface was exposed to vapors of PA. After post modification with PA, the surface pattern is similar to the one presented in Figure 38B. In the third step, this surface was illuminated with UV light once more using a second mask with 10 µm lines and 10 µm spaces which was oriented perpendicular to the first mask pattern. During this step, the Si-SCN and Si-PA stripes are illuminated partly. In this second UV illumination, the unexposed parts of the Si-PA stripes did not change significantly whereas the exposed parts of the Si-PA stripes changed to illuminated PA (Si-PAI) stripes. The remaining Si-SCN stripes were changed to alternating 10 µm patches of Si-SCN and Si-NCS.

Thus, on this resulting patterned surface there are four different surface terminations (SCN, NCS, PA and PAI). Their expected arrangement is sketched in Figure 44.

PA	PAI	PA	PAI	PA
SCN	NCS	SCN	NCS	SCN
PA	PAI	PA	PAI	PA
SCN	NCS	SCN	NCS	SCN
PA	PAI	PA	PAI	PA
SCN	NCS	SCN	NCS	SCN
PA	PAI	PA	PAI	PA

Figure 44: Expected resulting surface pattern after preparation processes.

Figure 45 presents the surface morphology and the friction image of the sample after the illumination and modification through the crossed masks.

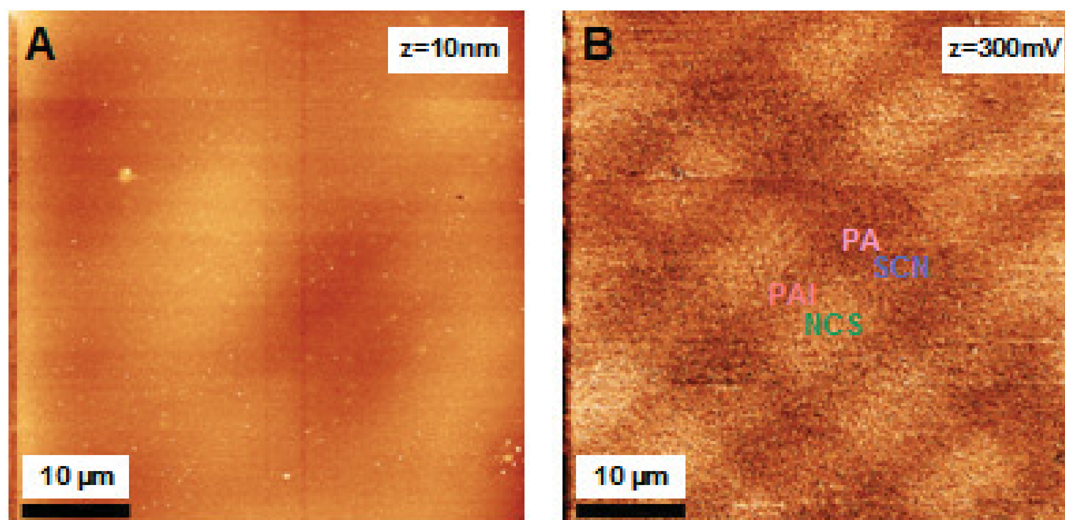

Figure 45: AFM results of the illuminated and modified Si-SCN surface layer after using two crossed 5 µm, and 10 µm masks, A) 50 µm×50 µm topography image with 10 nm z-scale; B) corresponding FFM image with a pattern of 5 µm×10 µm rectangular patches.

In the 50 µm×50 µm topography image (see Figure 45A), there are no structural features visible resulting from the patterning process. However, in the 50 µm×50 µm FFM image, a clear pattern of 5×10 μm^2 rectangle patches of four different shadings is detected. This is in agreement with the expected pattern of four different friction levels as shown in Figure 44. According to the friction contrast information obtained from the patterned samples described above, the chemical identification of these four different surface terminations is possible. In fact, in chapters 4.7 and 4.8, the puzzle will be solved which friction contrast is due to which surface termination.

3.3.6 Friction force contrast of an ester surface layer

Upon the illumination with UV light, the photoreactive organic surface layer consisting of acetic acid 4-(2-trichlorosilanyl-ethyl)-phenyl ester molecules undergoes a Photo-Fries rearrangement. Using a contact mask with equidistant 3 µm lines and 3 µm spaces in inert atmosphere (N_2) and then post-modified with the perflurobutyryl chloride in dry CH_2Cl_2 solution in an Ar filled glove box, a functionalized patterned structure, which is composed of the alternating surface termination stripes of the unmodified acetoxy group and the modified perfluorobutyryl group, was formed on this surface layer. At Graz University of Technology, the thickness of the acetic acid 4-(2-trichlorosilanyl-ethyl)-phenyl ester layer was determined by XRR measurements to be 1.6 nm, which is higher than the theoretical thickness of upright standing molecules (approximately 1.1 nm). The increased thickness is attributed to a crosslink

combination of the trichlorosilane groups in the presence of water which results in a multilayer growth (measured multilayer thickness is about 3.6 nm up to 8 nm) [15]. Figure 46 shows the corresponding FFM data. The FFM can clearly reveal the materials contrast between modified and unmodified regions of the patterned surface [13].

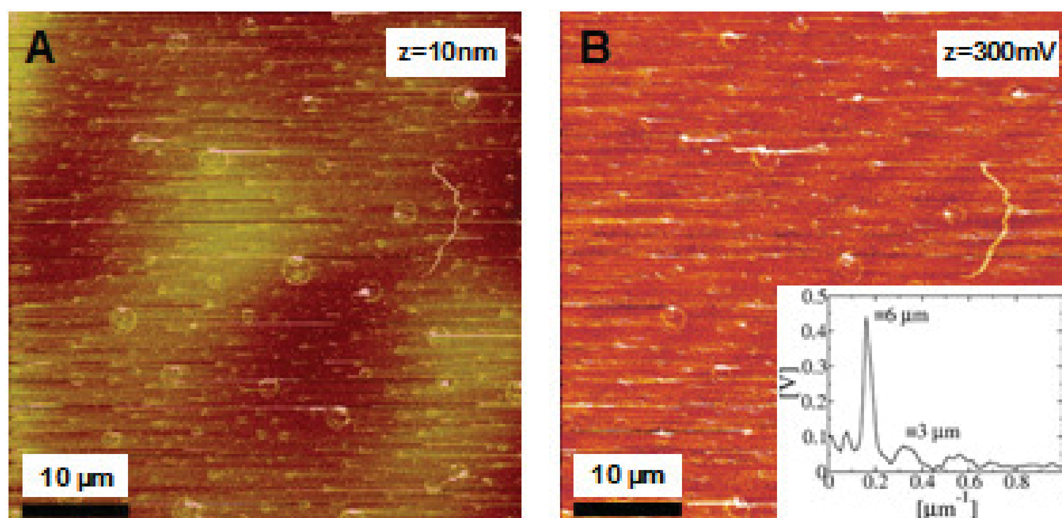

Figure 46: FFM image of the thin silane layer (8 nm) using a 3 µm mask (A: 50 µm×50 µm topography image with 10 nm z-scale; B: alternating 3 µm broad stripes pattern in FFM image; the inset in B shows a 1D-FFT perpendicular to the stripes calculated from the friction image).

In the 50 µm×50 µm topography image (Figure 46A), the homogeneous surface morphology with a lot of surface contamination can be distinguished although the multilayer is formed by a crosslink of the trichlorosilane head groups. There are no structural features resulting from the patterning process. This is due to the fact that the obtained height difference (estimated to be approximately 1 to 2 nm) after post modification by a lateral distance of 3 µm (periodicity of the mask) can hardly be analyzed in the FFM measurement.
However, the 3 µm wide alternating stripes of the two different friction level, which is in agreement with 3 µm contact mask spacing, can be detected in the 50 µm×50 µm friction image (z-scale = 300 mV, set point = 0.4 V). This demonstrates the power of the FFM analysis also for the case of photoreactive ester surface layers.
The inset in Figure 46B shows a one dimensional Fast Fourier Transformation (FFT) of the FFM image in a direction perpendicular to the stripes. Clear peaks in reciprocal space corresponding to 6 µm and 3 µm in real space demonstrate the high accuracy of the patterning technique [13].

4. Discussions and Conclusions

4.1 Influence of the plasma etching process on the substrate roughness

In the process of the surface pre-treatment, the plasma etching process has to be undertaken to get a hydrophilic surface with a high concentration of surface hydroxyl groups [11], which are needed to bind with the head groups of these organic molecules.

Analyzing AFM topography images of these three kinds of substrate surfaces investigated, the average rms roughness σ, lateral correlation length ξ and the roughness exponent α have been determined (see Table 1). The obtained roughness parameters are unchanged for substrate pre-treatment processes, which are without plasma etching and with 50 seconds or 150 seconds plasma etching times. Therefore, we conclude that the oxygen plasma etching process has no significant influence on the surface roughness.

Plasma etching time	σ (nm)	δ (nm)	α
0 second	0.2 ± 0.05	20	0.5
50 seconds	0.2 ± 0.05	30	0.5
150 seconds	0.2 ± 0.05	20	0.5

Table 1: Surface roughness results in different plasma etching time.

4.2 Influence of the substrate types on Si-SCN thin surface layer morphology

As described in chapters 2.1.1 and 3.3.2, there are two different types of substrates dedicated for different characterization: the Infineon type substrate is for FTIR Spectroscopy measurements and the Sigert type substrate is for XPS and XRR measurements.

According to AFM surface roughness results (rms roughness σ, lateral correlation length ξ and the roughness exponent α) in Table 2, it can be shown that different substrate types (Infineon / Sigert type) do not influence the surface layer morphology significantly, which is indeed desired. For this reason, both substrates are used for measurements and the results have been used side by side without further notice.

Substrate type	σ (nm)	ξ (nm)	α (nm)
Infineon type	0.3 ± 0.05	20	0.5
Sigert type	0.4 ± 0.05	15	0.5

Table 2: Surface roughness results of Si-SCN layer on 2 types of substrates.

4.3 Influence of the preparation processes on the morphology of the surface layer

The PFDTS surface layers are of less quality than the CSTS layers and have many small clusters on the surfaces. For PFDTS, the average PFDTS rms roughness σ is 0.4 nm. However, after wiping with a tissue, smoother surfaces can be obtained and the PFDTS rms roughness σ in the wiped band area is again comparable to the one of the substrate (σ = 0.3 nm), whereas sometimes the wiping traces are visible (see Figure 47). The smoothest PFDTS surface can be formed after Method 2 which is a wet chemical method in a glove box.

CSTS surface layers are very smooth (σ = 0.3 nm) and their surface roughness is similar to the one of the substrates. The smoothest CSTS surface is obtained after Method 1 and 2 which are wet chemical methods in a fume hood or a glove box, respectively.

Using AFM measurements, the different surface morphology and roughness after different fabrication methods can be characterized and compared. But the chemical quality of the surface can not be identified. Subsequent CA measurements therefore have been used to prove whether the PFDTS or CSTS surface layers really exist on the substrate (see chapter 3.2.2.3).

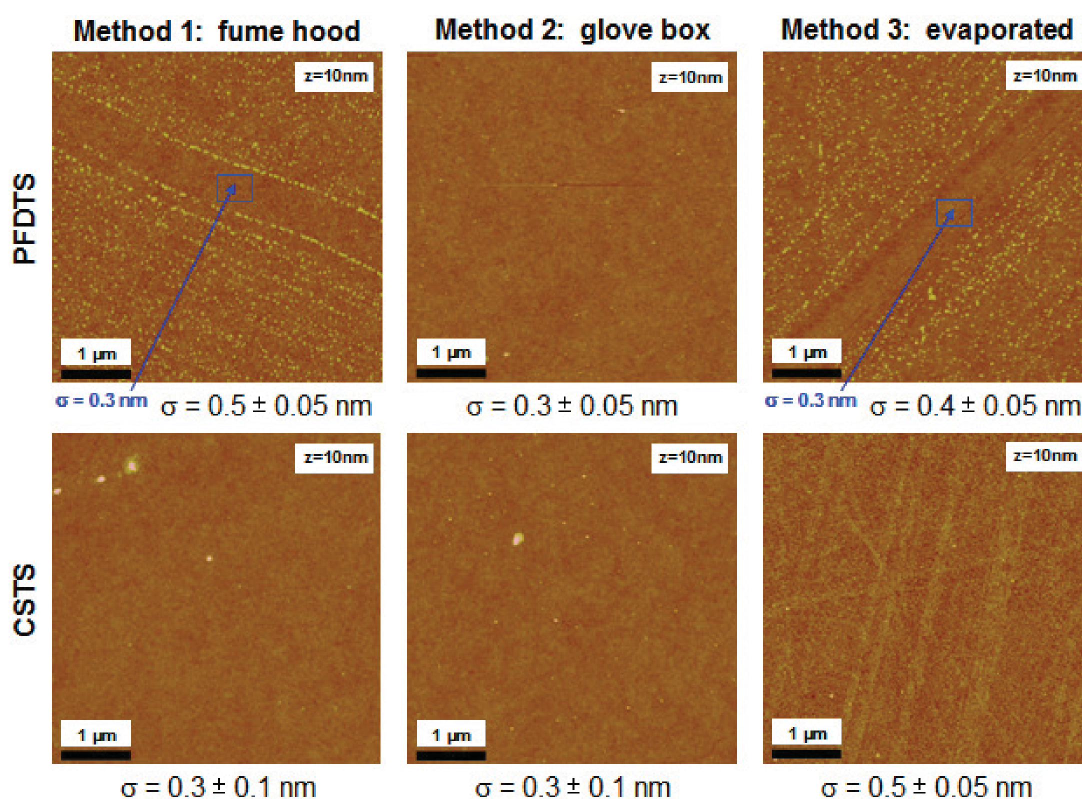

Figure 47: Comparison of the surface morphologies, obtained by AFM, between the CSTS and PFDTS surface layers after different methods. The rms values are indicated for each image. The blue arrows point to areas in the wiped strips, the corresponding σ values are given in blue.

In summary, according to the AFM measurements described in chapter 3.2.2, the PFDTS and CSTS surface layers formed by Method 2 have the best quality and their roughness is comparable to the one of the substrate (see Figure 47 and Table 3). Therefore, Method 2, using a glove box, is the best preparation method for both the PFDTS and the CSTS surface layers, since this preparation method 2 does not change surface morphology significantly.

surface	σ (Method 1) (nm)	σ (Method 2) (nm)	σ (Method 3) (nm)
PFDTS	0.5±0.05	0.3±0.05	0.4±0.05
CSTS	0.3±0.1	0.3±0.1	0.5±0.05
plasma etched substrate	0.2±0.05	0.2±0.05	0.2±0.05

Table 3: Surface roughness results for PFDTS and CSTS surface layers after different methods.

In Table 4, the CA of PFDTS and CSTS surface layer are given. Compared with the literature CA results (water CA of PFDTS = 110° [26]; water CA of CSTS = 87° [27]), the values of CSTS CA formed by Method 1 and 2 are much lower than the literature value of CSTS and are similar to the CA of the SiO_2 substrate (see Table 4). This means that most presumably Method 1 and 2 do not result in CSTS layers on the substrate surface. The CA of PFDTS after different methods is similar to the literature data and different from the substrate, which is a proof that PFDTS molecules really exist on the substrate surface.

surface	CA (Method 1)	CA (Method 2)	CA (Method 3)
PFDTS	99°	100°	101°
CSTS	33°	35°	79°
plasma etched substrate	40°	40°	40°

Table 4: CA comparison between the PFDTS, CSTS surface layers and their substrate surface by using H_2O ($\Theta_{(PFDTS\ literature)} = 110°$; $\Theta_{(CSTS\ literature)} = 87°$).

According to the AFM and CA results, for PFDTS surface layers, method 2 (in glove box) works best, since there is almost no influence on the surface morphology. For the CSTS layers, only method 3 (evaporated) resulted in the desired surface layer, however, with a significant increase in rms roughness.

4.4 Influence of deposition conditions on Si-SCN surface layer morphology

As found in chapter 3.3.1, during the surface layer deposition processes, the different Si-SCN solution concentration, deposition time, and sample orientation have different influences on the Si-SCN surface layer morphology.
According to the roughness results of lying and standing samples, there are no big

differences between higher concentration + longer deposition time and lower concentration + shorter deposition time. However, for the same concentration of solution and time of deposition, the standing sample method results in smoother surfaces than for the lying samples. This means that the deposition orientation in solution has significant influence on surface morphology (see Table 5). This can be explained as follows: in the Si-SCN solution, more molecules can easily deposit on the lying sample surface. The side deposition of the solution molecules on the standing sample surface is more difficult than the one on the lying sample, which leads to a low surface roughness.

depostion orientation	σ (nm)	ξ (nm)	α
lying sample	1.5 ± 0.05	20	0.5
standing sample	0.4 ± 0.05	15	0.5

Table 5: Surface roughness results of 2 samples with different deposition orientation in the same 0.1 vol% SCN-solution and 16 hours deposition time.

4.5 Influence of the Si-SCN layer preparation process on surface roughness

After pre-treatments of plasma etching and deionized water dip, the Infineon type SiO_2 substrates were immersed into a Si-SCN solution under ambient conditions to deposit a Si-SCN surface layer. The Si-SCN surface layer undergoes a photoisomerization to the corresponding Si-NCS surface layer upon illumination with UV light. After the photoisomerization process, the Si-NCS surface layer is modified with PA to form a Si-PA surface layer.

These layer preparation processes (Si-SCN layer deposition, photoisomerization and post modification) influence the surface roughness of the corresponding surface layer formed. Figure 48 presents three-dimensional AFM topography images (from substrate to post modified surface), which illustrate this influence of all film preparation processes on surface roughness. Homogeneous films of Si-SCN (Figure 48B), and PA modified Si-PA films (Figure 48C), were prepared and compared to the surface of the bare SiO_2 substrate (Figure 48A).

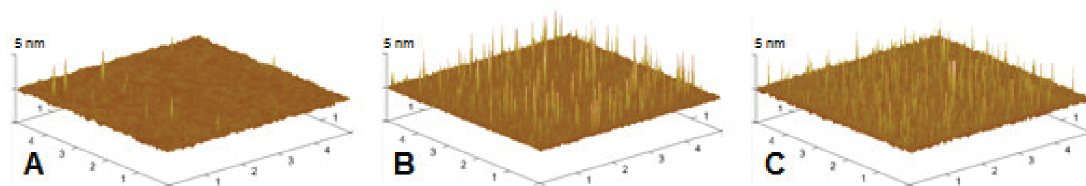

Figure 48: Three-dimensional AFM topography images of the 3 different surfaces after different preparation processes (A: SiO_2 substrate surface; B: Si-SCN surface; C: post modified Si-PA surface).

The surface of the substrate (Figure 48A) shows a uniform featureless topography as expected for a silicon oxide surface. The rms roughness of $\sigma = 0.2\pm0.05$ nm, the

lateral correlation length ξ = 30 nm, and the roughness exponent α = 0.5 confirm the qualitative observation. Deposition of a thin layer of Si-SCN shown in Figure 48B leads to a slight increase in the rms roughness $\sigma = 0.3 \pm 0.05$ nm, ξ = 15 nm, and α = 0.5. Modifying the surface with vapor of PA (Figure 48C) does not lead to a further increase in rms roughness ($\sigma = 0.3 \pm 0.05$ nm, ξ = 25 nm and α = 0.5) (see Table 6).

surface layer	σ (nm)	ξ (nm)	α
SiO_2 substrate	0.2 ± 0.05	30	0.5
Si-SCN	0.3 ± 0.05	15	0.5
Si-PA	0.3 ± 0.05	25	0.5

Table 6: Surface roughness results of 4 differently prepared surfaces.

4.6 Influence of post modifications on Si-SCN surface layer morphology

According to the surface information acquired in chapter 3.3.3, by AFM and CA measurements (see summary given in Table 7), it can be concluded that the photoisomerization and post modifications do not change the surface roughness significantly. Looking in more detail at the data it can be seen that the UV illumination and post modifications with two different reactants (PA or NH_3) have slight influence on the surface free energy.

surface	σ (nm)	ξ (nm)	α	α_{water}	$\alpha_{water / toluene}$	IFT_D	IFT_P	IFT total
Si-SCN	0.3 ± 0.05	15	0.5	73°	87°	24.0	3.5	27.5
Si-PA	0.3 ± 0.05	25	0.5	73°	90°	29.2	1.3	30.5
$Si-NH_3$	0.3 ± 0.05	35	0.5	73°	89°	30.9	0.7	31.6

Table 7: Surface data of Si-SCN (without illumination), Si-PA (Si-SCN with illumination and post modification with PA), and $Si-NH_3$ (Si-SCN with illumination and post modification with NH_3) surface layers.

4.7 Identification of two surface terminations on the stripe pattern by FFM

In FFM, the torsion of the cantilever is sensitive to different surface terminations on the surface. Therefore, a visualization of patterned surfaces should be possible because the interaction of the tip should be different with SCN and PA terminations. For lithographically patterned photoreactive surface layers, the identification of different surface terminations in FFM measurement is very important. Clear structural features in the topography image and the correspondence between the topography and the friction image are the keys to distinguish the different terminations on the surface. In FFM images of the (Si-NCS/Si-PA) patterned surface (see Figure 49) the stripe pattern can be detected in both topography and friction image.

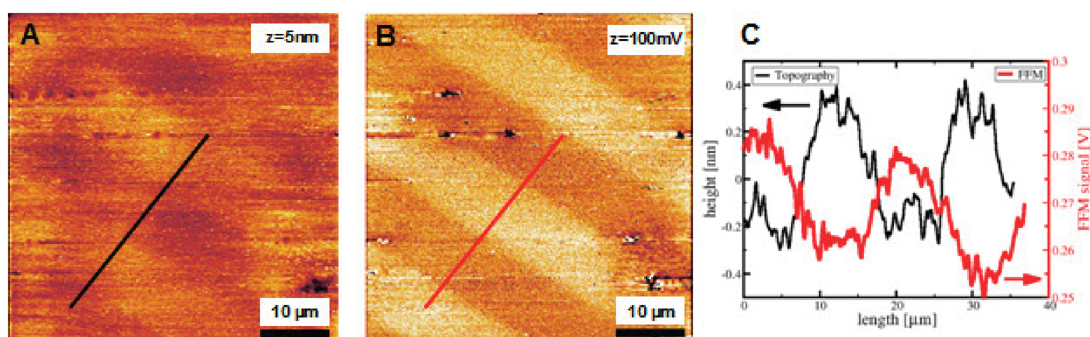

Figure 49: Alternating stripes of SCN and PA termination group in 50 µm×50 µm FFM images (B) with 5 nm z-scale by using a 10 µm wide mask (A: topography image; C: cross section of one lineal position in both topography and friction image, which shows PA stripes are roughly 0.5 nm higher than SCN stripes (from [3]).

From the combined cross section in Figure 49C the height difference between the Si-SCN stripes and Si-PA stripes is determined to be 0.5 nm. The addition of an alkyl group to the molecule due to the post modification with PA is expected to result in an increase of the Si-PA stripe thickness. In chapter 2.2.2.1.4 it has been mentioned that the yield after the post modification (from Si-SCN to Si-PA) is approximately 30% because only 30% Si-NCS can be formed from Si-SCN in the photoreaction [6]. Therefore, a total increase in volume (and thickness) by 30% after post modification with PA can be expected. According to the discussion above, an increase in Si-PA stripe thickness by about 10%, which corresponds to 0.5 nm height difference, is reasonable. That means, the Si-PA stripes are by about 0.5 nm higher than the Si-SCN stripes in the topography image.

Because of the interference of real morphology undulations and surface contamination, in 50 µm×50 µm topographical image (z-scale = 5 nm) only a weak stripe pattern with the expected 10 µm spacing can be detected. Clear 10 µm wide alternating stripes of two different friction levels are distinguishable in the 50 µm×50 µm friction image (z-scale = 100 mV, set point = 0.3 V). The stripe pattern in the friction image corresponds to the stripe pattern in the topography image. According to this correspondence between the topography and friction image, both Si-SCN and Si-PA stripes can easily be identified: the low stripes in the topography image correspond to the bright stripes (higher friction) in the friction image and the higher stripes in the topography image correspond to the dark stripes (lower friction) in the friction image. Since the Si-PA stripes are higher than Si-SCN stripes this means that the friction coefficient of the modified PA termination is smaller than the one of the unmodified SCN termination (height in the topography image: Si-PA > Si-SCN; friction force in the friction image: Si-PA < Si-SCN).

Thus, FFM proves in this case that the patterning process by partial illumination using a mask and subsequent post modification of the illuminated stripes is possible and leads to a chemical functionalized pattern on the surface. Here, FFM is able to clearly distinguish the two terminations on the patterned surface.

4.8 Identification of four surface terminations on the patterned surface by FFM

As reported in chapter 3.3.6, the patterned surface was formed by two UV illuminations using two different crossed masks with an intermediate post modification step with PA. In Figure 50, the friction contrast pattern of 5×10 μm^2 rectangle patches of four different shadings, which correspond to different friction levels, is shown again. Although there are no structural features resulting from the patterning process in the topography image, we can also here identify these four surface terminations on the patterned surface by using the previously obtained friction contrast results. From chapter 4.7, the hierarchy (friction coefficient: Si-PA < Si-SCN) is known. With additional knowledge of the positions of the terminations in the pattern, the observed friction contrast of the four surface terminations (SCN, NCS, PA and PAI) can be ordered in the following way.

There are only two possible friction contrast sequences due to the position restriction of this regular pattern (PA and NCS rectangles can not occur in the same stripe), which is NCS > PAI ≧ SCN > PA or PA > SCN ≧ PAI > NCS. Due to the previous friction contrast result PA < SCN, the NCS > PAI ≧ SCN > PA is the only solution of the friction level. Therefore, in our approach the hierarchy of friction force of at least three surface terminations (Friction coefficient: PA < SCN < NCS) can be determined (see Figure 50).

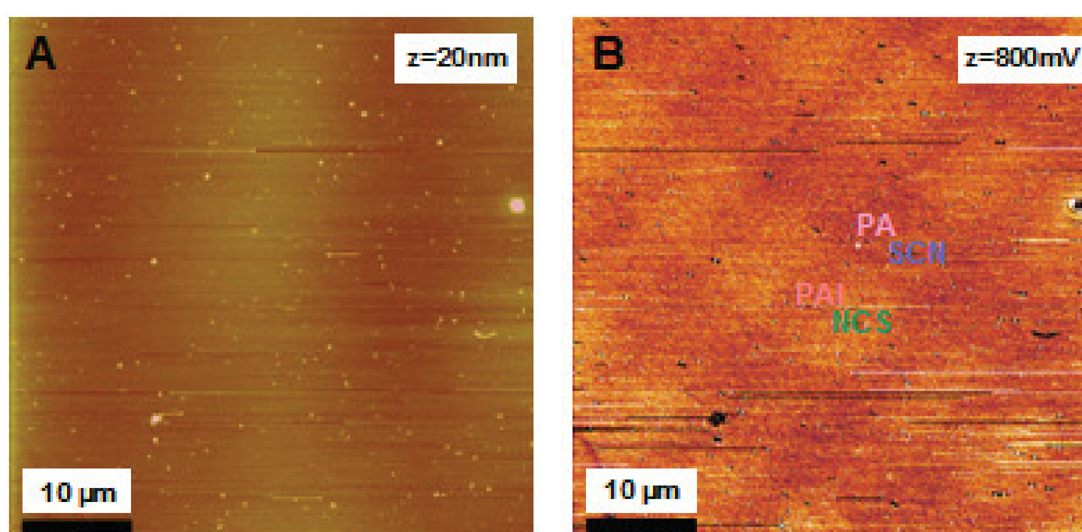

Figure 50: FFM results of the illuminated and modified Si-SCN surface layer after using two crossed 5 µm, and 10 µm masks (A: 50 µm×50 µm topographic image with 20 nm z-scale; B: friction image with the different terminations indicated).

According to the resulting hierarchy of friction forces of the three surface terminations (Friction coefficient: PA < SCN < NCS), the rectangular patches of four different shadings can be identified: the highest tip-film interaction and therefore the largest friction is observed for NCS termination in the brightest rectangular patches and the smallest friction is for the PA termination in the darkest rectangular patches. The SCN termination is located in the 5 µm stripes neighboring the NCS termination.

As different terminations of surface molecules have different interaction with the tip, FFM allows revealing chemical patterns inscribed by a photolithographic process into a photoreactive surface layer. In this approach, at least three different chemical surface terminations could be simultaneously identified.

4.9 Influence of termination polarity and stiffness on friction force

A possible explanation for the resulting hierarchy of friction forces of the three surface terminations (Friction coefficient: PA < SCN < NCS) can be given by the different polarity of the individual terminations on the surface (SCN, NCS, PA) and by the stiffness of the molecular surface terminations [3].
Comparing the data on the dipole moment and surface tension of ethyl isothiocyanate and ethyl thiocyanate (see Table 8), it can be found that the ethyl isothiocyanate (which is similar to the isothiocyanate NCS termination) has a higher polarity than the corresponding ethyl thiocyanate (which is similar to the thiocyanate SCN termination) [28]. That means the friction force between the silicon tip, which is covered with a native oxide layer, and the surface can increase with the polarity of the surface. Therefore, through the UV illumination a higher friction force can be recorded on the NCS stripes (which have higher surface polarity) than on the non-illuminated SCN stripes. In Table 8 it is seen that the difference in surface free energy between the two terminations (ethyl isothiocyanate and ethyl thiocyanate), which correspond to the NCS and SCN terminations, is only 1.2 mN/m. This is the reason why the friction contrast between the Si-NCS and Si-SCN stripes is rather poor.

surface molecule	dipole moment [Debye]	surface tension γ [mN/m]
ethyl thiocyanate	3.33	34.8
ethyl isothiocyanate	3.67	36.0

Table 8: Dipole moments and surface tensions of similar surface termination groups (from [29]).

After the modification with the PA, the NCS termination changes to the non-polar PA termination on the surface so that the friction force of the PA termination is lower than the one of the NCS and SCN terminations. Therefore, this surface polarity explanation (surface polarity: PA < SCN < NCS) is totally corresponding to the hierarchy sequence of friction force of surface terminations (friction coefficient: PA < SCN < NCS).
Also, the stiffness of the surface termination molecule can influence the surface friction force [29, 30]. The friction force of the termination can increase with the stiffness of the surface termination molecule. The molecule of the PA surface termination is flexible so that it can reduce the friction by bending under the applied normal load. Compared with the PA termination, the shorter and stiffer SCN and NCS terminations cannot bend under the normal load (Si-NCS has two double bonds between sulfur, carbon, and nitrogen; Si-SCN has a triple bond between carbon and

nitrogen while the sulfur is linked by two single bonds) [3]. Therefore, the stiffness explanation of the surface termination (termination molecular stiffness: PA < SCN and NCS) is corresponding to the hierarchy of friction forces of surface terminations (friction coefficient: PA < SCN and NCS).

4.10 Final discussion of the applicability of FFM measurements

FFM measurements are performed in contact mode. Due to the corresponding lateral forces, the tip rubs the surface at all times and some surface molecules (termination molecules of the organic surface layer) can be removed or rubbed out (see Figure 51). Therefore, the FFM measurements can lead to local damage either on the surface layer or on the tip or even on both. Such an example is presented in Figure 51.

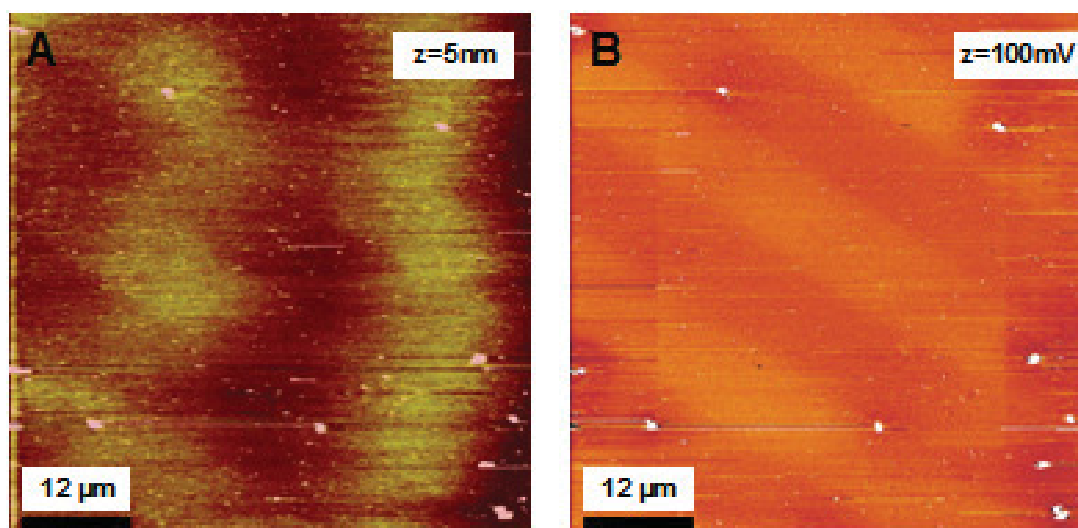

Figure 51: FFM results of a twice scanned surface layer with PA and SCN terminations (10 µm wide mask) (A: 60 µm×60 µm topography image with 5 nm z-scale; B: friction image).

After illumination with UV light and post modification with PA, the SCN termination group is changed to the PA one. This PA termination layer was scanned twice in the same surface position with different scanning size:

In the first step, the surface is scanned in FFM mode with 40 µm×40 µm scan size and then in the second step it is scanned with a larger 60 µm×60 µm size at the same position. In the friction images, it is easy to find the 40 µm×40 µm square area of the first scan, in which the friction contrast is slightly different compared to the area outside this square. This means that, after the first scanning, the PA termination layer changed slightly by the rubbing tip. Thus, the scanning of the tip on the surface can remove or rub out the surface molecules slightly or even significantly. The effect will depend on the applied normal force related to the friction force. The degree of surface damaging can be enhanced by increasing surface contaminations and morphological undulations as will be shown below.

Otherwise, the atomic-scale variation (local spatial shift) of topography and friction [31] can not be detected in our FFM measurements because our surfaces are smooth and there are not very strong morphology interferences on it.

1) The influence of the surface contamination

The scanning probe microscope tip on a surface represents a single asperity contact. When the tip encounters a contamination during the scanning, the surface molecules, which adsorb on the tip, will fall from the tip onto the surface and will be moved by the scanning tip. The moving trace can be detected in the FFM images (see Figures 52). Therefore, surface contaminations can cause disturbances of the image.

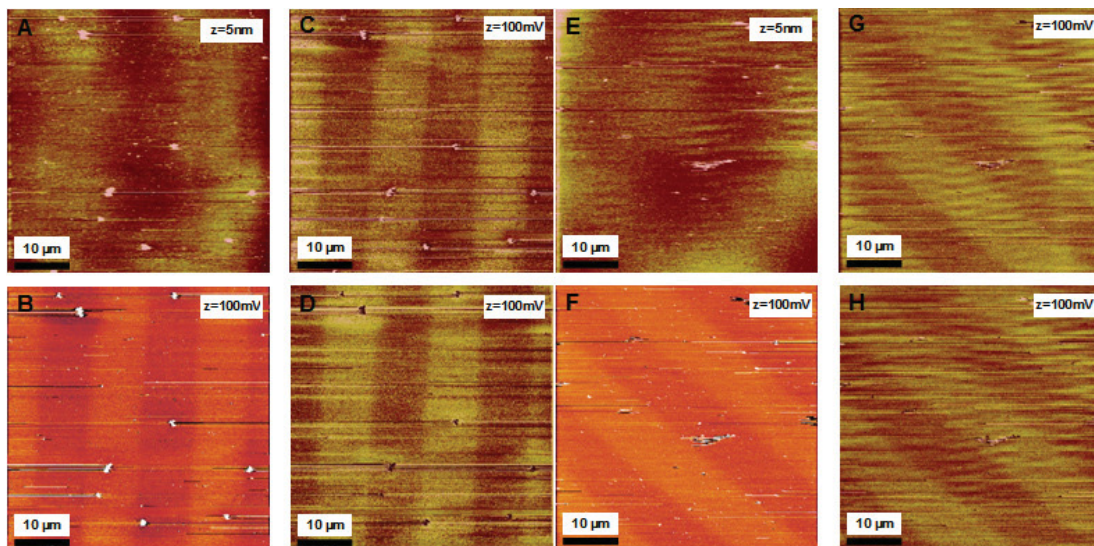

Figure 52: Collection of AFM data (topography and friction) for surfaces with many contaminations on a patterned surface layer using 10 µm mask (Si-SCN surface modified with PA: A) topography image, B) real friction image, C) friction image in trace direction, D) friction image in retrace direction; Si-SCN surface modified with FA: E) topography image, F) real friction image, G) friction image in trace direction, H) friction image in retrace direction). The contaminations lead to many removing traces of the surface molecules in the friction images.

2) The influence of the morphological undulations

Due to interference with morphology changes, the friction contrast pattern in the friction images are not real and clear. This morphological interference can be removed by a subsequent mathematical method ((trace FFM data – retrace FFM data) / 2). The real friction image formed by this method can show the real friction contrast on the surface without the surface topographical interference.

An example is a polymer (polynorbonene) thin film on the silicon oxide substrate, which is illuminated with UV light by using a 10 µm wide mask and then modified with acetyl to form a functional termination layer. A very strong surface corrugation (30 nm) is detected in the topography image and there are also alternating 10 µm wide stripes in the friction images. But the corresponding stripes in both friction images are

not of opposite contrast, which means that there is no true friction contrast on the surface. Indeed, the friction image reveals that there is no friction contrast on the surface (see Figure 53B). The interpretation of the formation of these alternating friction contrast stripes in the friction images is the superposition with the topographical undulation.

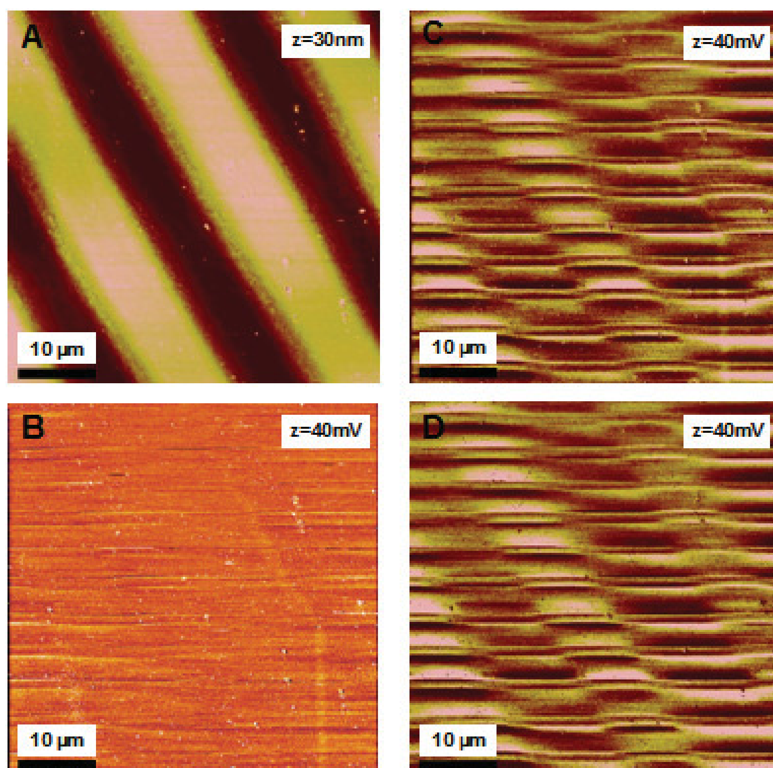

Figure 53: Strong influence of the topographical undulation on the friction images of a polymer surface.

Through the real friction image, the interference of the topographical undulation on the friction images can be eliminated. The real friction contrast pattern in both trace and retrace friction images must be opposite correspondingly.

In fact, our subtraction operation can here not eliminate the topography-induced effect due to the ratchet mechanism of friction [32, 33]. The subtraction operation can only reduce the topography interference. However, in our case, the topography undulations are not very strong but smooth. Therefore, we can use this subtraction operation to reduce almost all the interference of surface morphology (see Figure 53B).

5. Summary and outlook

This contribution was concerned with the precise morphology characterization of organic thin surface layers (PHDTS and CSTS) – which was carried out using atomic force microscopy – and with the material-induced micro-scale friction investigation of the photoreactive thin surface layer (Si-SCN and ester layer) using friction force microscopy. The understanding of the surface roughness and frictional properties on the nanometer scale is essential for these studies. Thus, atomic force microscopy based investigations were well suited for these investigations. Roughness parameters (rms roughness σ, lateral correlation length ξ, and roughness parameter α) were utilized to describe the surface roughness quantitatively. Introduction to the single-asperity-contact friction mechanism was given and a subtraction operation of the friction images to reduce morphology induced artifacts was applied. Furthermore, different chemical processes - which relate to surface plasma etching, layer deposition methods, surface photoisomerization and modification – were described. In addition, detailed materials information (composition, molecule length, surface contact angle, etc.) of these organic surface layers were provided.
The first part of the investigations was dedicated to thin PHDTS and CSTS films grown on SiO_2 for OTFT applications. Using AFM for topography imaging, we investigated various samples, which differed in wiping processes and chemical preparation methods. The topography images associated with surface parameters (σ, ξ and α) were recorded to depict film surface qualities after different physical and chemical preparation processes. The topographic AFM analysis shows that the wiping process can effectively reduce rms roughness of thin film surfaces from 3.6±0.8 nm to 0.3±0.1 nm, but can also wipe off the entire thin film from the substrate, especially in the case of the CSTS layer. Therefore, compared with literature value of CA, the contact angle measurements were applied to find out whether the thin film really exists on the substrate. According to the AFM and CA results, the PFDTS surface layers formed by the Method 1 (in a glove box) have the best quality and the roughness is comparable to the one of the substrate, which means that there is almost no influence on the surface morphology. For the CSTS surface layers, only the Method 3 (evaporated) resulted in the desired surface layer on the substrate despite of a significant increase in rms roughness.
The second type of organic thin films under investigation were novel photosensitive Si-SCN and ester surface layers, which can easily be isomerized by UV light and subsequently modified to form a functionalized patterned surface. Using AFM for morphology characterization, samples which varied with different SiO_2 substrate types, deposition conditions and chemical preparation processes were measured. According to results of roughness parameters recorded, it has been proven that there is no influence of the substrate type on the surface morphology. Preparation with the same concentration of solution and time of deposition, the surfaces of standing samples (σ = 0.4±0.05 nm) are smoother than the lying samples (σ = 1.5±0.05 nm). This means that the orientation of the sample during deposition in solution has

significant influence on the surface morphology. During surface layer preparations, the multi-step chemical processes result in a slight change of the surface roughness. Depositing the Si-SCN layer, the rms roughness of Si-SCN surface is 0.3±0.05 nm, which is higher than the one on the SiO_2 substrate (σ = 0.2±0.05 nm). There is no evident change of layer roughness in the course of UV illumination and subsequent modification of the surface layer. On these modified patterned surfaces, different terminations of surface molecules have different interactions with the tip. Using FFM, it is possible to study very sensitively frictional properties under low force and at a small length. The topography and friction images were recorded simultaneously to find relationships between them. In the friction image clear frictional stripes - which were formed by partial illumination of photoreactive surface layers using a mask and subsequent post modification - were detected, which prove that this patterning process works and can result in a functionalized surface pattern. Meanwhile, we compared the image of the topography with the friction image. Careful comparison of the corresponding topographical and frictional signals can be assisted to identify different chemical surface terminations in our approaches. On a special patterned surface using a crossed mask, the hierarchy of friction (friction coefficients: PA < SCN < NCS) of at least three surface terminations can be identified simultaneously.

In conclusion, we can state that the AFM/FFM combination provides high spatial resolution and superior sensitivity to adhesion forces for researching the organic surface layers. FFM in combination with other methods (XRR, XPS, CA measurements, etc.) is a suitable tool to reveal the surface tribological properties on a very small scale.

In our future plan, high resolution AFM research will be continued. On the patterned surfaces, quantitative measurement of the adhesion force is in progress using the Varenberg method [34]. To enhance FFM contrast, measurements with functionalized AFM tips [35] are planned. Because there are still many problems left unresolved in friction theories, especially in macro-tribology theory which are not suitable to explain the friction mechanisms in nano- and micro-scales [33], further friction measurements with light load and on the nano-scale will be necessary for understanding more about the complex friction behaviors. With respect to the CA studies, measurements with an additional (non polar) liquid are planned to determine the surface free energies. In addition, other auxiliary AFM techniques will be implemented to study the organic thin film in our measurements. In order to investigate crystallographic domains in thin organic films, Transverse Shear Force Microscopy (TSM) [36] will be used and adjusted to determine the domain size. Kelvin Probe Force Microscopy (KPFM) [37] as well as conductive Atomic Force Microscopy (C-AFM) [38] will be utilized to obtain the work function of surfaces and information on conductivity at atomic or molecular scale, respectively.

6 References

[1] W. Brütting, Physics of Organic Semiconductors, WILEY-VCH Verlag GmbH & Co. KGaA, Weinheim, 2005, Page 1.
[2] G. Hlawacek, P. Puschnig, P. Frank, A. Winkler, C. Ambrosch-Drax, and C. Teichert, Science 321, 108 (2008).
[3] G. Hlawacek, Q. Shen, C. Teichert, A. Lex, G. Trimmel, and W. Kern, Chem. Phys. 130, 044703 (2009).
[4] P. Pacher, A. Lex, V. Proschek, O. Werzer, P. Frank, S. Temmel, W. Kern, R. Resel, A. Winkler, C. Slugovc, R. Schennach, G. Trimmel, and E. Zojer, J. Phys. Chem. 111, 12407 (2007).
[5] K. P. Pernstich, S. Haas, D. Oberhoff, C. Goldmann, D. J. Gundlach, B. Batlogg, A. N. Rashid, and G.. Schitter, J. Appl. Phys. 96, 6431 (2004).
[6] A. Lex, P. Pacher, O. Werzer, A. Track, Q. Shen, R. Schennach, G. Koller, G. Hlawacek, E. Zojer, R. Resel, M. Ramsey, C. Terchert, W. Kern, and G. Trimmel, Chem. Mater. 20, 2009 (2008).
[7] T. Griesser, T. Hoefler, S. Temmel, W. Kern, and G. Trimmel, Chem. Mater. 19, 3011 (2007).
[8] A. Ulman, Chem. Rev. 96, 1533 (1996).
[9] H. Sellers, A, Ulman, Y. Shnidman, and J. E. Eilers, J. Am. Chem. Soc. 115, 9389 (1993).
[10] (a) G. Weiqiang, D. J. Abdallah, and R. G. Weiss, J. Photochem. Photobiol. A: Chem. 139, 79 (2001). (b) R. A. Finnegan, and D. Knutson, Tetrahedron Lett. 9, 3429 (1968).
[11] P. Pacher, A. Lex, V. Proschek, H. Etschmaier, E. Tchernychova, M. Setzen, U. Scherf, W. Grogger, G. Trimmel, C. Slugovc, and E. Zojer, Adv. Mater. 20, 3143 (2008).
[12] A. Glaser, J. Foisner, H. Hoffmann, and G. Friedbacher, Langmuir 20, 5599 (2004).
[13] T. Hoefler, A. Track, P. Pacher, Q. Shen, H. Flesch, A. Lex, G. Hlawacek, G. Koller, M. Ramsey, R. Schennach, R. Resel, E. Zojer, C. Teichert, W. Kern, G. Trimmel, and T. Griesser, submitted to Materials Chemistry and Physics.
[14] A. Lex, Dissertation, Graz University of Technology, 2008.
[15] Y. Wang, and M. Lieberman, Langmuir 19, 1159 (2003).
[16] V. J. Morris, A. R. Kirby, A. P. Gunning, Atomic Force Microscopy for Biologists, Imperial College Press, London, UK, 2004, Page 5.
[17] K. S. Birdi, Scanning Probe Microscopes - Applications in Science and Technology, CRC Press, Boca Raton, Florida, USA, 2003, Page 17.
[18] http://www.nanosensors.com/products_overview.html#PPP.
[19] Y. Zhao, G. Wang, T. Lu, Characterization of Amorphous and Crystalline Rough Surface: Principles and Applications, Academic Press, San Diego, CA, USA, 2001, Pages 7-42.
[20] C. Frisbie, L. Rozsnyai, A. Noy, M. Wrighton, and C. Lieber, Science 265, 2071

(1994).
[21] V. N. Koinkar, and B. Bhushan, J. Vac. Sci. Technol. A, 14, 2378 (1996).
[22] V. N. Koinkar, and B. Bhushan, J. Appl. Phys. 81, 6, 2472 (1997).
[23] Sara Shieh, An Analysis of Contact Angle Measurement, March, 2001.
[24] D. Owens, and R. Wendt, J. Appl. Polym. Sci. 13, 1741 (1969).
[25] T. Kavc, G. Langer, P. Pölt, K. Reichmann, and W. Kern, Macromol. Chem. Phys. 203,1099 (2002).
[26] S. Fleith, A. Ponche, R. Bareille, J. Amedee, and M. Nardin, Colloids Surf. B. 44, 15 (2005).
[27] K. Wu, T. C. Bailey, C. G. Willson, and J. G. Ekerdt, Langmuir 21, 11795 (2005).
[28] J. A. Dean, Lange's Handbook of Chemistry, McGraw-Hill Press, New York, USA, 1999.
[29] B. Bhushan, and H. Liu, Phys. Rev. B, 63, 245412 (2001).
[30] R. Overney, E. Meyer, J. Frommer, D. Brodbeck, R. Lüthi, L. Howald, H.-J. Güntherodt, M. Fujihira, H. Takano, and Y. Gotoh, Nature (London), 359, 133 (1992).
[31] B. Bhushan, Wear 259, 1507 (2005).
[32] S. Sudararajan, and B. Bhushan, J. Appl. Phys. 88, 8 (2000).
[33] S. Achanta, T. Liskiewicz, D. Drees, and J. P. Celis, Tribol. Int. 10, 1016 (2009).
[34] M. Varenberg, I. Etsion, and G. Halperin, Rev. Sci. Instrum. 74, 3362 (2003).
[35] M. Ruths, Langmuir 19, 6788 (2003).
[36] J. A. Last, and M. D. Ward, Adv. Mater. 8, 730 (1996).
[37] F. Krok, K. Sajewicz, J. Konior, M. Goryl, P. Piatkowski, and M. Szymonski, Phys. Rev. B. 77, 235427 (2008).
[38] S. Kremmer, C. Teichert, E. Pischler, H. Gold, F. Kuchar, and M. Schatzmayr, Surf. Interface Anal. 33, 168 (2002).

7 List of Abbreviations

AFM	Atomic Force Microscopy
CA	Contact Angle
C-AFM	Conductive Atomic Force Microscopy
CFM	Chemical Force Microscopy
CSTS	2-(4-Chlorosulfonylphenyl) ethyltrichlorosilane
DI	Digital Instruments
FA	trifluorethylamin (fluorinated amine)
FFM	Friction Force Microscopy
FTIR	Fourier Transform Infrared
HHCF	Height-Height Correlation Function
HPLC-grade	High Performance Liquid Chromatography Grade
IFT	interfacial tension
IFT_D	dispersive interfacial tension
IFT_P	polar interfacial tension
KPFM	Kelvin Probe Force Microscopy
LFM	Lateral Force Microscopy
NCS	isothiocyanate
OLEDs	Organic Light Emitting Diodes
OTFTs	Organic Thin Film Transistors
PA	prophylamine (thiourea compound)
PFDTS	(Heptadecafluoro-1,1,2,2-tetrahydrodecyl) trichlorosilane
PSD	Position-sensitive Photodiode
rms	root mean square
SAM	self-assembled monolayer
SCN	thiocyanate
Si-SCN	(4-thiocyanatomethyl) phenyltrimethoxysilane
Si-PAI	illuminated PA
THF	Tetrahydrofuran
TSM	Transverse Shear Force Microscopy
XPS	X-ray Photoelectron Spectroscopy
XRR	X-ray Reflection

8 Appendixes

Overview of the samples measured

Sample name	Molecule name	Sample file name	Sample remark	Sample producer
Si50pa	SiO_x	50pa.000-005	Si+50 nm SiO_2 (plasma etching)	A.Lex
Si150pa	SiO_x	150pa.000-008	Si+150 nm SiO_2 (plasma etching)	A.Lex
50SiO	SiO_x	50SiO.000-003	Si+50 nm SiO_2	A.Lex
150SiO	SiO_x	150SiO.000-002	Si+150 nm SiO_2	A.Lex
SiO50	SiO_x	sio50.000-004	Si+50 nm SiO_2	A.Lex
SiO50pa	SiO_x	sio50pa.000-005	Si+50 nm SiO_2 (plasma etching)	A.Lex
SiO150pa	SiO_x	sio150pa.000-005	Si+150 nm SiO_2 (plasma etching)	A.Lex
Si-plasma	SiO_x	si_plasma.000-003	plasma etching	A.Lex
SAM1-HDTS	HDTS	sam1_hexadecyl.000-002		A.Lex
SAM2-HDTS	HDTS	sam2_hexadecyl.000-001		A.Lex
Perflour-Abzug	PFDTS	Perflour_Abzug.000-010	in fume hood	A.Lex
Perflour-Box	PFDTS	perflour_box.000-010	in glovebox	A.Lex
Perflour-Aufgedampft	PFDTS	perfluor_aufgedampft.000-004	evaporated	A.Lex
SAM-perflour	PFDTS	sam_perfluor.000-008		A.Lex
CSTS-Abzug	CSTS	chlorsulfon_abzug.000-006	in fume hood	A.Lex
CSTS-Box	CSTS	chlorsulfon_box.000-006	in glovebox	A.Lex
CSTS-Aufgedampft	CSTS	chlorsulfon_aufgedampft.000-008	evaporated	A.Lex
SAM-CSTS	CSTS	sam_chlorsulfon.000-009		A.Lex
AFM01	PFDTS	pfdts_gb.000-014	in glovebox	A. Lex
AFM02	CSTS	csts_gb.000-009	in glovebox	A. Lex
AFM03	HDTS	hdts_gb.000-007	in glovebox	A. Lex
AFM04	SCN	scn_gb.000-008	in glovebox	A. Lex
AFM05	Nb	nb_sam_plasma.000-007	plasma etching	A. Lex
AFM06	SCN	scn_nolicht.000-005	no illumination	A. Lex
AFM07	SCN	scn_licht_grid.000-022	illumination with PA (mask)	A. Lex
AFM08	Nb	nb_sam_cs.000-009	Caroscher acid	A. Lex
AFM09	SCN	scn_sam_gb1w.000-010	1 week	A. Lex
AFM10	SCN	scn_nl_afm10.000-005	no illumination	A. Lex
AFM11	SCN	scn_lg-afm11.000-004	illumination with	A. Lex

			NH_3 (mask)	
AFM12	SCN	scn_nl_afm12.000-005	no illumination	A. Lex
AFM13	SCN	scn_lg-afm13.000-008	illumination with PA (square mask)	A. Lex
AFM14	PFDTS	pfdts_afm14.000-002	in glovebox	A. Lex
AFM15	PFDTS	pfdts_afm15.000	in glovebox	A. Lex
AFM16	SCN	scn_nl_afm16.000-007	no illumination	A. Lex
AFM17	SCN	scn_l_afm17.000-004	illumination with PA	A. Lex
AFM18	SCN	scn_nlb_afm18.000-004	no illumination	A. Lex
AFM19	SCN	scn_lg-afm19.000-009	Illumination (square mask)	A. Lex
AFM20	SCN	scn_lg-afm20.000-010	illumination with PA (square mask)	A. Lex
AFM21	SCN	scn_l_pa_afm21.000-007	illumination with PA (square mask)	A. Lex
AFM22	SCN	scn_l_f_afm22.000-006	illumination with FA (square mask)	A. Lex
AFM23	SCN	scn_nl_afm23.000-007	no illumination	A. Lex
AFM24	SCN	scn_l_pa3_afm24.000-011	illumination with PA (3 µm mask)	A. Lex
AFM25	SCN	scn_l_pa10_afm25.000-013	illumination with PA (10 µm mask)	A. Lex
AFM26	SCN	scn_l_pa_afm26.000-001	illumination with PA	A. Lex
AFM27	SCN	scn_l_fa3_afm27.000-007	illumination with FA (3 µm mask)	A. Lex
AFM28	SCN	scn_l_fa10_afm28.000-003	illumination with FA (10 µm mask)	A. Lex
AFM29	SCN	scn_l_fa_afm29.000	illumination with FA	A. Lex
AFM30	SCN	scn_nl_afm30.000-001	no illumination	A. Lex
AFM31	SCN	scn_l_3_afm31.000	Illumination (3 µm mask)	A. Lex
AFM32	SCN	scn_l_10_afm32.000-004	illumination (10 µm mask)	A. Lex
AFM33	SCN	scn_l_fa10k_afm33.000	illumination with FA (10 µm mask)	A. Lex
AFM34	SCN	scn_l_5_afm34.000-004	illumination (5 µm mask)	A. Lex
AFM35	SCN	scn_l_pa5_afm35.000-002	illumination with PA (5 µm mask)	A. Lex
AFM36	SCN	scn_l_fa5_afm36.000-008	illumination with	A. Lex

			FA (5 µm mask)	
AFM37	SCN	scn_l_pa3l5_afm37.000-004	Twice illumination with PA (3×5 µm crossed mask)	A. Lex
AFM38	SCN	scn_l_pa3fa5_afm38.000-003	twice illumination with PA and FA (3×5 µm crossed mask)	A. Lex
AFM39	SCN	afm39_alex_gekeutzt.000-002	twice illumination with PA (10×5 µm crossed mask)	A. Lex
AFM40	SCN	afm40_alex_gekeutzt.000-002	twice illumination with PA (10×5 µm crossed mask)	A. Lex
AFM43	SCN	ffm43_gekreuzt_5pa_10il.000-002	twice illumination with PA (10×5 µm crossed mask)	A. Lex
neuAFM01	TSEP	tsep_nl_neuafm1.000-008	no illumination	T.Höfler
neuAFM02	TSEP	tcsep_l_10_neuafm02.000-002	illumination (10 µm mask)	T.Höfler
neuAFM03	TSEP	tsep_l_dphh10_neuafm03.000-004	illumination and modification (10 µm mask)	T.Höfler
neuAFM04a	TSEP	tsep_l_ac2_neuafm4a.000-006	illumination and modification	T.Höfler
neuAFM04b	TSEP	tsep_l_ac1_neuafm4b.000-001	illumination and modification	T.Höfler
FFM14	TSEP	ffm14_hoefler_acetic_f12.000-002	illumination with perflurobutyryl (10 µm mask)	T.Höfler
FFM15	TSEP	ffm15_hoefler_a12.000-002	illumination with acetyl(10 µm mask)	T.Höfler
FFM16	TSEP	ffm16_hoefler_a16.000-002	illumination with acetyl(10 µm mask)	T.Höfler
FFM17	TSEP	ffm17_hoefler_f16.000-002	illumination with perflurobutyryl (10 µm mask)	T.Höfler
FFM18	TSEP	ffm18_hoefler_f3mju.000-002	illumination with perflurobutyryl (10 µm mask)	T.Höfler
FFM19	TSEP	ffm19_hoefler_f5mju.000-002	illumination with perflurobutyryl (5 µm mask)	T.Höfler
FFM20	TSEP	ffm20_hoefler_f10mju.000-002	illumination with	T.Höfler

			perflurobutyryl (3 µm mask)	
FFM21	TSEP	ffm21_hoefler_f3mju.000-002	illumination with perflurobutyryl (3 µm mask)	T.Höfler
FFM22	TSEP	ffm22_hoefler_f5mju.000-002	illumination with perflurobutyryl (5 µm mask)	T.Höfler
FFM23	TSEP	ffm23_hoefler_f5mjul.000	illumination with perflurobutyryl (5 µm mask)	T.Höfler
FFMP1	Polymer	ffmp1_hoefler.000-001	illumination with heptafluorobutyryl (5 µm mask)	T.Höfler
FFMP2	Polymer	ffmp2_hoefler.000-003	illumination with acetyl (2 µm mask)	T.Höfler
FFMP3	Polymer	ffmp3_hoefler.000-001	illumination with heptafluorobutyryl (2 µm mask)	T.Höfler
FFMP4	Polymer	ffmp4_hoefler_3mju.000-004	illumination with acetyl (3 µm mask)	T.Höfler
FFMP5	Polymer	ffmp5_hoefler_5mju.000-007	illumination with acetyl (5 µm mask)	T.Höfler
FFM01-UB	TSEP	ffm01_griesser_b.000-004 afm01_griesser_b.000	illumination	T. Grießer
FFM01-1F	TSEP	ffm01_griesser_f.000-005 afm01_griesser_f.000	illumination and modification	T. Grießer
FFM02-UB	TSEP	ffm02_griesser_b.000-003	illumination	T. Grießer
FFM02-1F	TSEP	ffm02_griesser_f.000-004 afm02_griesser_f.000	illumination and modification	T. Grießer